

LA-UR: 04-4530

# Evolution and Yields of Extremely Metal Poor Intermediate Mass Stars

Falk Herwig

*Los Alamos National Laboratory, Los Alamos, NM 87544*

`fherwig@lanl.gov`

*Department of Physics and Astronomy, University of Victoria, 3800 Finnerty Rd, Victoria, BC, V8P 1A1*

## ABSTRACT

Intermediate mass stellar evolution tracks from the main sequence to the tip of the AGB for five initial masses (2 to 6  $M_{\odot}$ ) and metallicity  $Z=0.0001$  have been computed. The detailed 1D structure and evolution models include exponential overshooting, mass loss and a detailed nucleosynthesis network with updated nuclear reaction rates. The network includes a two-particle heavy neutron sink for approximating neutron density in the He-shell flash. It is shown how the neutron-capture nucleosynthesis is important in models of very low metallicity for the formation of light neutron-heavy species, like sodium or the heavy neon and magnesium isotopes. The models have high resolution, as required for modeling the third dredge-up. All sequences have been followed from the pre-main sequence to the end of the AGB when all envelope mass is lost. Detailed structural and chemical model properties as well as yields are presented. This set of stellar models is based on standard assumptions and updated input physics. It can be confronted with observations of extremely-metal poor stars and may be used to assess the role of AGB stars in the origin of abundance anomalies of some Globular Cluster members of correspondingly low metallicity.

*Subject headings:* stars: AGB — stars: evolution — nuclear reactions, nucleosynthesis, abundances — stars: interiors

## 1. Introduction

The chemical production of low- and intermediate mass stars during their asymptotic giant branch phase of evolution is an important contribution to the galactic chemical evolution. For example, half of all elements heavier than mass number  $A = 90$  are made in low mass AGB stars by the  $s$ -process. AGB stars are responsible for a significant fraction of the carbon in the solar system abundance mix. AGB stars are the favored candidate for the main primary nitrogen source at lower metallicity (Pettini et al. 2002). The discrepancy of observations and galactic chemical evolution predictions based on massive star yields is in particular evident for some neutron heavy isotopes of certain elements (like Mg or Na, Timmes et al. 1995). This indicates the role of very low metallicity AGB stars to the early galactic chemical evolution. Equally important are the informations obtained from an increasing number of spectroscopic observations of extremely metal-poor (EMP) stars.

In the past yield predictions for a range of initial masses and metallicities have been derived from so-called synthetic AGB models (Renzini & Voli 1981; Marigo et al. 1996; van den Hoek & Groenewegen 1997). In these models the evolution is described by constructing fitting formulas to certain quantities of full stellar evolution models that solve the full set of stellar structure and nuclear energy generation. The most recent improvements include a full envelope integration for the hot bottom burning phase of massive AGB stars (Marigo 1998). The synthetic AGB model approach is very well justified under certain circumstances and for specific purposes. The computation of AGB stellar models requires high numerical resolution and significant computing time. In the past large grids in mass and metallicity with several ten- to onehundredthousand models for each sequence have not been feasible due to their computationally demanding nature. This is changing now and as an example, Karakas et al. (2002) have presented a comprehensive grid of AGB calculations to study differentially the dependence of DUP on mass and metallicity. Still, full stellar evolution models in the past were not able to reproduce, for example, the third dredge-up (DUP) in a way that agrees with observations. New results from nuclear physics may help to resolve this issue in the future (Herwig & Austin 2004). Synthetic models on the other hand can parameterize the third DUP in some way, and calibrate its efficiency with observed properties of AGB stars, for example using the C-star luminosity function of the Magellanic Clouds. The synthetic model predictions are therefore internally consistent with observations. In addition these models are useful because they condense the information contained in the C-star LF, or in C-rich star and O-rich star number counts in the Magellanic Clouds into more simple constraints, which detailed structure and evolution models have to reproduce. For example, the synthetic models by Marigo et al. (1996) require that efficient dredge-up must take place at core masses as low as  $0.58 M_{\odot}$ , a value which has even been revised downward by a more recent update (Marigo et al. 1999).

In order to model yields and the abundance evolution for EMP stars full stellar models appear to be in particular important. We are just beginning to identify the peculiarities of nucleosynthesis in EMP AGB stars (or at  $Z=0$  should they have existed, Chieffi et al. 2001). Synthetic models rely both on accurate structure and evolution models to derive the fitting formulas, as well as on a good calibration. Both are presently not well established at metallicities of  $Z < 0.001$ . Models of massive AGB stars at very low metallicity for example, show behaviors not seen in models of larger metallicity, like H-burning during the DUP or DUP reaching below the He-shell (Herwig 2004). It is therefore not appropriate to simply extrapolate synthetic models that have been calibrated at moderate metal deficiency to very low metallicities. In order to improve the situation more complete stellar evolution calculations are needed. Here, the structure and chemical evolution for a set of five tracks with masses from  $2 M_{\odot}$  to  $6 M_{\odot}$  at metallicity  $Z = 0.0001$  are presented.

The application of these models may include comparison to observations of EMP stars or tests of the possible role IMS (intermediate mass stars) in the chemical evolution of low-metallicity Globular Clusters. Although the grid is far from complete in mass and metallicity the calculations may be useful for Galactic Chemical Evolution models. Since the structural evolution is given as well, the models may be used to investigate the s-process.

In Paper I (Herwig 2004) the evolution of massive AGB stars at very low metallicity has been described in detail, in particular the interplay of hot bottom burning and the *hot* DUP. In another previous paper we have specifically addressed the possible implications of the more massive cases at this metallicity for the star-to-star abundance variations observed in globular clusters (Denissenkov & Herwig 2003). Here the detailed thermodynamic, structural and abundance evolution of a homogeneous set of intermediate mass EMP stellar models is presented. In § 2 the code changes compared to the version used in Paper I are described. The model results are given in § 3. The conclusions are presented in § 4.

## 2. Physical input, stellar evolution code and model calculations

The stellar evolution code and all model assumptions are the same as in Paper I, with the following exceptions.

### 2.1. Mass loss

Mass loss for AGB stars of very low metallicity is neither observationally nor theoretically well constrained, and one has to rely on extrapolation from larger metallicities and

rather qualitative and indirect considerations. For a mass loss formula both the functional dependence of mass loss on stellar parameters as well as the absolute calibration are needed.

Mass loss rates of Mira-like pulsating stars can be calculated by modeling the dynamical structure and evolution of their atmospheres (Bowen 1988). For solar-like metallicity Blöcker (1995) has extracted the luminosity dependence of the Bowen (1988) models and finds

$$\log \dot{M} \propto 3.7 \log L. \quad (1)$$

The physical input like the opacities as well as the properties of dust formation of the dynamical atmosphere models depend on the metallicities. However, no such models are available for low or very low  $Z$ . Here I assume not only that Eq.(1) can be applied at  $Z = 10^{-4}$ , but also that it approximately applies to changes in  $L$  due to changes in  $Z$  too. This assumption may in fact not be entirely foolish. The DUP is more efficient in EMP AGB stars (Herwig 2004, and § 3) and the CNO elements collectively reach close to the solar value abundances in the envelope. A comparison of the Rosseland mean opacity for a  $3 M_{\odot}$  TP-AGB model at  $Z = 0.02$  and  $Z = 10^{-4}$  yields a difference of typically less than 10% for  $\log T < 4.6$ .

If the dependence Eq. (1) is applied to luminosity variation due to varying metallicity, then the variation of stellar parameters with metallicity introduces a significant variation of the mass loss. In fact due to this effect one obtains a larger mass loss at lower  $Z$  because the luminosity is larger at lower  $Z$ . The average luminosity and temperature of a  $2 M_{\odot}$  and a  $5 M_{\odot}$  for a range of metallicities is shown in Fig. 1. From these stellar structure and evolution results one determines approximately

$$\log L \propto -0.2 \log Z. \quad (2)$$

Together with Eq. (1) this implies that  $\dot{M}(Z = 10^{-4}) \sim \eta_1 \cdot \dot{M}(Z = 0.02)$  with  $\eta_1 \sim 50$ .

van Loon (2000) has attempted to derive a mass loss-metallicity relation based on observations of Magellanic Cloud giants, and suggests that

$$\log \dot{M} \propto 0.3 \log Z. \quad (3)$$

This exponent has a very large uncertainty, mainly due to small-number statistics. Due to its observational nature Eq. (3) contains both the possible dependence of Eq. (1) on metallicity and the dependence of stellar parameters on metallicity (Eq. 2). Tentatively extrapolating the relation of van Loon (2000) to  $Z = 10^{-4}$  the absolute mass loss rates at  $Z = 0.02$  and  $Z = 10^{-4}$  are related by  $\dot{M}(Z = 10^{-4}) \sim \eta_2 \cdot \dot{M}(Z = 0.02)$  with  $\eta_2 \sim 0.2$ .

One can then obtain a calibration for the Bowen-Bloeker mass loss rate (Eq. 1) at  $Z = 10^{-4}$  by  $\eta_B = \eta_2 / \eta_1$  which gives  $\eta_B = 0.004$  for the exponent 0.3 of Eq. (3). However, it

has been mentioned that this exponent is subject to large uncertainty. In particular, both result for M stars and for C stars are compatible with  $\log \dot{M} \propto -0.3 \log Z$  which implies  $\eta_2 \sim 5$ . Therefore the largest mass loss at  $Z = 10^{-4}$  within this framework is  $\eta_B = 0.1$  and this is the adopted value for the present study. In this way these calculations give a lower limit to the envelope enrichment and the corresponding yields. A lower mass loss rate would lead to a longer TP-AGB duration with more TPs and subsequent DUP events.

## 2.2. Overshooting

The treatment of convective boundaries, both at the bottom of the envelope convection as well as at the bottom of the pulse-driven convection zone (PDCZ) during the He-shell flash effects stellar models in many ways, including the dredge-up predictions. The consequences and implications of various treatments of mixing at these convective boundaries has been explored in detail (Herwig et al. 1997; Mowlavi 1999; Herwig 2000; Langer et al. 1999; Lugaro et al. 2003; Herwig et al. 2003; Herwig 2004). Models which include an adjustable amount of depth- and time-dependent amount of overshooting at all convective boundaries show efficient dredge-up at low core-masses.

The same concept of exponential overshooting as in Paper I is applied. For the TP-AGB models the overshoot efficiency at the bottom of the PDCZ is set to  $f_{\text{PDCZ}} = 0.008$  while the efficiency at the bottom of the convective envelope is set to  $f_{\text{CE}} = 0.016$  at all times. Models with larger  $f_{\text{PDCZ}}$  have higher temperature for the  $^{22}\text{Ne}$  neutron source. Lugaro et al. (2003) found that if  $f_{\text{PDCZ}}$  is too large some s-process branchings produce isotopic ratios that are irreconcilable with laboratory measurements in pre-solar SiC grains. For example, the branching at  $^{95}\text{Zr}$  is sensitive to the temperature at the bottom of the He-shell flash convection zone. If  $f_{\text{PDCZ}}$  is too large the temperature is too large and the predicted  $^{96}\text{Zr}/^{94}\text{Zr}$  ratio is larger than measured in the grains. Lugaro et al. (2003) have concluded that  $f_{\text{PDCZ}} = 0.016$  may be too large. Unfortunately the neutron cross section of the unstable isotope  $^{95}\text{Zr}$  is very uncertain. The current range of estimates differ within a factor of four (Kawano, priv. com., Bao et al. 2000a; Jorissen & Goriely 2001), and a more conclusive analysis has to await a better experimental determination of this cross section. Other nuclear reaction rates as studied by Herwig & Austin (2004) may also be important. In any case the concept of overshooting at the bottom of the PDCZ plays an important role in currently favored models of H-deficient central stars of planetary nebulae (of spectral type PG1159 and [WC]-CSPN, Koesterke & Hamann 1997; Dreizler et al. 1996; Werner & Herwig 2005).

The rather small value for  $f_{\text{CE}} = 0.016$  can not reproduce the partial mixing needed

for the  $^{13}\text{C}$  neutron source in low mass TP-AGB stars (Goriely & Mowlavi 2000; Herwig et al. 2003). One can estimate the mass of the s-process layer resulting from partial mixing that reproduces the observed stellar s-process overabundances. The stellar model must accomplish such an enrichment within a number of dredge-up events that can be constrained by observations. This number can be derived from model comparison with the observed C-star luminosity function and the observed ratio of C-stars to O-rich AGB stars (Marigo et al. 1999). In particular newer synthetic models including the effect of C/O ratio dependent molecular opacities (Marigo 2002) indicate that typical low-mass AGB stars that produce the s-process elements may in fact experience only five to at most ten thermal pulses and subsequent dredge-up events during the C-rich phase.

In the context of evaluating the properties of rotating AGB star models Herwig et al. (2003) estimated that the partial mixing zone that hosts the s-process nucleosynthesis should have a mass  $M_{\text{P}} > 7 \cdot 10^{-5} M_{\odot}$ , in agreement with more detailed calculations. Exponential overshooting as applied here with an efficiency  $f_{\text{CE}} = 0.016$  leads to a partial mixing zone with a mass  $\approx 10^{-6} M_{\odot}$  only (Herwig 2000; Herwig et al. 2003). In a detailed analysis Lugardo et al. (2003) have assumed that  $f_{\text{CE}} = 0.128$  and obtained overall overabundance factors close to what is observed. There are indications that  $f_{\text{CE}}$  may be even larger in the framework of the *s*-process partial-mixing concept, at least for solar-metallicity cases.

However, in Paper I it was shown that in models of extremely low metallicity even a very small amount of exponential overshooting leads to *hot DUP* with potentially very significant implications to the overall evolution. In these stars the  $^{12}\text{C}$  rich intershell material beneath the proton-rich matter is hotter than in cases with higher metallicity. If protons are forced into the  $^{12}\text{C}$  rich core during the dredge-up phase of the TP cycle they are burnt vigorously. The additional H-burning luminosity can further drive convective instability and cause a corrosive, convective H-shell that thus penetrates much deeper into the core than without this additional H-burning. This *hot DUP* and the resulting corrosive burning is in fact conceptually related to the conductive propagation of nuclear flames considered in ONeMg cores in the context of SN Type Ia models (Timmes et al. 1994).

In Paper I calculations of a  $5 M_{\odot}$  dredge-up phase with  $f_{\text{CE}} = 0.03$  – about twice as large as the value assumed here – prompted ongoing dredge-up that would have terminated the AGB in approximately 2000 yr (based on some uncertain assumptions on mass loss for such configurations). The situation for lower-mass cases may be less dramatic, but still hot DUP may alter the conditions for the formation of a partial mixing zone at extremely low metallicity, as enhanced H-burning during this phase would result from any efficient convection-driven extra-mixing process.

While it is possible that exponential extra-mixing as assumed in the diffusive over-

shooting approach is responsible for the *s*-process partial mixing zone at solar metallicity, the situation is rather unclear at extremely low metallicity. The situation can be improved by investigating how the structure (i.e. mainly the DUP depth) depends on the interplay of extra-mixing and hot DUP, and how extra-mixing itself is effected by nuclear burning in the overshooting layer. In these calculations a rather small efficiency of overshooting is assumed. This way most of the complications caused by hot DUP are avoided. However, the nuclear production predictions do not include the uncertain effect of a more extended  $^{13}\text{C}$  pocket.

### 2.3. Nuclear network

The updated nuclear reaction network includes all relevant charged particle reactions,  $\beta$ -decays and neutron-capture reactions. If available the NACRE reaction rates are used (Table 1). The nuclear network solution is based on rates from linear interpolations in the 250 grid point logarithmic tables generated by the WWW database tool *NETGEN* (Jorissen & Goriely 2001). For the calculation of the energy generation in the stellar structure solution a smaller network containing the dominating CNO cycle, pp-chain, and He-burning reactions has been used. The reaction rates have been calculated from the fitting formulas to the NACRE reactions (Angulo et al. 1999), which provide smooth T-derivatives. Potentially this dual approach may introduce an inconsistency because a small amount of energy released by trace elements may be ignored, and because the fitting formulas may disagree with the tabulated values by a few percent. However, it turns out that the fitting formula (despite the published fitting errors) represent the tabulated values very well for the most important H- and He-burning reactions in the relevant temperature range.

All important light n-capture reactions as well as the several Fe-group species capturing neutrons are included. A light and a heavy n-sink take care of the remaining n-capture species as in Herwig et al. (2003). The two-particle sink approximating the trans-iron species allows a rough estimate on the number of neutrons captured per iron seed particle ( $n_{\text{cap}}$ ) which is an important diagnostic tool for the *s*-process. For the sink-cross sections the same value as in Herwig et al. (2003) is taken. This cross section depends on the heavy elements abundance distribution, and therefore a cross section derived for (near-)solar metallicity is not correct at very low metallicity. However, a detailed study of the *s*-process at very low metallicity which is required to estimate an appropriate sink-cross section is not available at this time. In addition the exact value of the heavy sink-cross section is less important at very low metallicity because the role of heavy species for the determination of the neutron density is smaller when large amounts of primary light n-capture species, like  $^{22}\text{Ne}$ , are present.

### 3. Results

#### 3.1. Structural evolution

The average structural properties of the model grid are summarized in Table 2. It shows how the stellar parameters as well as evolutionary times change systematically as a function of initial mass.

The surface temperature of the models as a function of TP-phase and mass changes only little, and all TP-AGB models are in the range  $T_{\text{eff}} = 4000 - 4350$  K. All sequences show very efficient third dredge-up. Therefore the core masses are on average almost constant during the TP-AGB evolution. These full stellar evolution models do not support the scenario of low-mass supernovae in the early Galactic halo proposed by Zijlstra (2004). An important assumptions in this proposal is that the cores of IMS stars are able to grow to the Chandrasekhar mass because the mass loss is very low at low metallicity. The models presented here can not rule out this proposal, but it is fair to say that they do at least raise some serious doubts. Deep dredge-up events prevent the core from growing. They also cause substantial pollution of the surface layers with C, N and O, all of which are important sources of opacity in the outer stellar layers. Thus the assumption that mass loss is in fact negligible in these stars may not be correct. Finally, the hot DUP (previous section and Paper I) is more effective at higher core mass. Thus, from these calculations I have more reasons to doubt rather than believe this idea.

The stellar luminosity and radius evolve only little with TP number and during a TP cycle. Averaged values are given in Table 2. These TP-AGB models with initial masses of  $2 \dots 6 M_{\odot}$  have core masses in the range  $0.62 \dots 1.05 M_{\odot}$ . The luminosities follow approximately an exponential core-mass luminosity relation:

$$\log L / L_{\odot} = 1.7414 \times M_c / M_{\odot} + 2.8799 \quad (4)$$

This is shown in Fig. 2, where in addition two data points for TP-AGB stars (last TP cycle) of zero-metallicity by Chieffi et al. (2001) are shown. Our models show sharp luminosity and radius peaks during the first deep dredge-up events (see Paper I for details). These peaks may be important if the binary evolution and of EMP stars (in the CH-star scenario) is considered. It may be that interaction or enhanced tidal synchronization occurs preferentially during these spikes close to the time of the He-shell flash.

The core mass is defined here as the mass within which the hydrogen mass fraction is  $X_H < 0.37$ . The core mass grows because of H-shell burning. The recurrent third dredge-up events decrease the core mass. The result is a characteristic saw-tooth shaped curve of the core-mass as a function of time. In Fig. 3 the core mass evolution is shown for all sequences.

The DUP parameter is defined as  $\lambda = \Delta M_{\text{H}} / \Delta M_{\text{DUP}}$ , where  $\Delta M_{\text{H}}$  is the core mass growth due to H-burning during the interpulse phase. In all sequences  $\lambda \sim 1$  for the majority of TPs. Models with larger core mass have a shorter interpulse phase and smaller intershell layers (see Table 2), as it is the case at larger metallicity. For the mass loss law chosen here the more massive models experience more DUP events during which less processed material is mixed into the surface. This in addition to the larger dilution factor of the massive AGB stars due to their larger envelope mass, leads to the prediction that more massive AGB stars will generally have smaller overproduction factors, for example for the overall enrichment in the sum of CNO elements.

In addition to the mixing properties the temperatures at the nuclear production sites determine the chemical enrichment of the stars. In Table 3 the temperatures in the H-shell, the He-shell as well as the temperature at the bottom of the envelope convection and the bottom of the PDCZ are given. The temperature in the He-shell and the temperature at the bottom of the envelope convection zone vary substantially and the values given in the table should be considered typical numbers taken approximately when half of the interpulse phase has passed. The last line for each sequence gives the core mass and envelope mass when the computations have been stopped. The subsequent evolution would lead into the post-AGB and central star of planetary nebula phase of evolution. The sequences have been stopped before this numerically difficult transition phase away from the AGB starts, but after enough envelope mass has been lost for reliable yield predictions.

The density at the bottom of the PDCZ ranges from  $4.0 \times 10^3 \text{ g/cm}^3$  to  $4.8 \times 10^4 \text{ g/cm}^3$  for the  $2 M_{\odot}$  sequence (E82) while slightly lower densities are encountered at higher core masses ( $2 \times 10^3 - 1.8 \times 10^4 \text{ g/cm}^3$  for the  $6 M_{\odot}$  sequence E86).

### 3.2. Chemical evolution and yields

In the context of Galactic Chemical Evolution different species evolve differently as a function of metallicity (time) and depending on their particular location. In order to choose initial abundances for the stellar evolution models one can either adopt theoretical initial abundances from published galactic chemical evolution models (Timmes et al. 1995), or the initial composition is tailored to reproduce observed abundances at  $[\text{Fe}/\text{H}] = -2.3$ . Unfortunately, both approaches lead to different results for some important species (like N or Na), while the theoretical models can not be checked in other cases (like  $^{22}\text{Ne}$ ). Fortunately the yields of many important species of TP-AGB stars are dominated by primary nucleosynthesis production. Moderate uncertainties in the initial abundances will have only little effect on the results. This is certainly true for the CNO elements. Therefore, the initial composi-

tion is set to metallicity scaled solar abundance distribution. The largest difference between the initial metallicity at  $Z = 10^{-4}$  and a solar-scaled initial composition would concern the light elements deuterium and  $^3\text{He}$ . These should be overabundant at very low metallicity compared to the solar-scaled values due to big bang nucleosynthesis (Walker et al. 1991). In this study the light elements lithium and  $^3\text{He}$  are not considered.

IMS experience several kinds of dredge-up events that generate overabundances in their envelopes. At extremely low metallicity the second dredge-up after the end of core He-burning plays a more important role than the first dredge-up after the core H-burning. In fact in this model set only the  $2 M_{\odot}$  sequence has a first dredge-up that is deeper than the second dredge-up. The most massive cases do not even have a first dredge-up and Red Giant Branch evolution phase (Girardi et al. 1996). He-core burning sets in before the model star reaches the giant branch and temporarily reverses that evolution (Fig. 4). After that they evolve directly into early AGB stars and the envelope becomes convectively unstable for the first time. Although the repeated third dredge-up events are mainly responsible for the total chemical envelope enrichment with nucleosynthesis products it is nevertheless important to document the pollution during the evolution prior to the thermal pulse AGB.

The overabundances just before the first dredge-up event of the thermal pulse AGB evolution (Fig. 5) reflect mostly abundance changes that are secondary in nature. The  $^{12}\text{C}$  abundance is in all but the  $6 M_{\odot}$  case depleted by mixing the partially CN cycled envelope. Accordingly the  $^{14}\text{N}$  abundance is enhanced. In the  $6 M_{\odot}$  sequence the He-shell is hot and broad enough after the end of He-core burning that the descending envelope convection (second dredge-up) engulfs a small amount of primary  $^{12}\text{C}$ . This explains also other small CNO abundance differences between the  $6 M_{\odot}$  and the less massive cases. The Ne-Al isotopes are effected by secondary p-capture nucleosynthesis as well. This is more so the case for larger masses. In particular  $^{23}\text{Na}$  is produced from p-captures on Ne isotopes. For this element the production prior to the TP-AGB is significant compared to the later production during the TP phase if a solar-scaled  $^{22}\text{Ne}$  initial abundance is assumed. However, this may not be correct since standard models of massive stars (the yields of which may dominate the initial abundance distribution of EMP low- and intermediate mass stars) predict a lower than solar-scaled  $^{22}\text{Ne}$  abundance.

To compare the overall abundance evolution as a function of mass the envelope mass averaged mass fractions have been computed for each sequence and each species  $i$  using

$$X_{\text{av}}^i = \frac{1}{M_i - M_f} \int_{M_f}^{M_i} X^i(m) \, dm \quad (5)$$

where  $M_i$  and  $M_f$  are the stellar mass at the beginning and the end of the AGB evolution phase, and  $X$  is the surface mass fraction at a given time corresponding to the stellar mass.

These averaged abundances in the matter returned to the interstellar medium together with the adopted initial abundance distribution is given in Table 4. These averaged overabundances should be useful for comparison with trends in observed abundances of metal poor globular clusters or extremely metal-poor halo stars. Note that the squared bracket notation  $[X/\text{Fe}]$  is very well approximated by  $\log X_{\text{av}}/X_{\text{ini}}$  because the initial abundance is solar-scaled. The average overabundances are displayed for all cases in Fig. 6. Yields according to

$$p_i = - \int_{M_f}^{M_i} (X_i(m) - X_{\text{ini}}) \, dm, \quad (6)$$

are given in Table 5<sup>1</sup>.

The evolution of surface abundances and stellar parameters for all tracks is provided in abbreviated online tables (see Table 6 for a sample). A graphical representation is given in Fig. 7 to 10. For the following discussion two abbreviations are useful: *LC* refers to the low-mass cases 2 and  $3 M_{\odot}$  which do not experience hot-bottom burning, while *HC* refers to the  $4\text{-}6 M_{\odot}$  cases in which HBB is efficient.

**Helium**  $^4\text{He}$  is brought into the envelope by all dredge-up episodes. In addition HBB in HCs transforms H into helium. HCs are more efficient  $^4\text{He}$  producers than LCs, both in terms of the yields as well as the average abundance in the ejecta. The relative importance of the different production mechanisms is a function of initial mass. HCs generate the vast majority of  $^4\text{He}$  during the second dredge-up. Although HBB is most efficient in the most massive cases the  $6 M_{\odot}$  sequence (E0086), for example, generates only a few percent of the total  $^4\text{He}$  overabundance during the TP-AGB phase. Contrary, the  $2 M_{\odot}$  case (E0082) produces about two thirds of its  $^4\text{He}$  overabundance during the TP-AGB by third dredge-up. The mass dependence of the  $^4\text{He}$  yields suggests that for a Salpeter-like intial mass function both HCs and LCs are equally important producers of  $^4\text{He}$ .

**Carbon**  $^{12}\text{C}$  is produced in the He-shell by the triple- $\alpha$  reaction and dredged-up after the TP. The LCs show larger  $^{12}\text{C}$  overabundances and also larger yields then the HCs. The deeper dredge-up (in mass, not in dredge-up parameter  $\lambda$ ) and the smaller dilution factor due to a smaller envelope mass outweigh the fact that LCs have less TPs than HCs.  $^{13}\text{C}$  is not produced or destroyed in the  $2 M_{\odot}$  case which does not have HBB. The matter which is dredged-up from the intershell is void of  $^{13}\text{C}$  beacuse of the large  $^{13}\text{C}(\alpha, n)^{16}\text{O}$  cross-section. For this mass the overabundance is entirely secondary and stems from the pre-TP-AGB

---

<sup>1</sup>Table 5 available online.

evolution. For larger masses HBB becomes more and more important and so does the  $^{13}\text{C}$  overabundance, which is primary in these cases and exceeds the enrichment level obtained by the second dredge-up. For  $M \geq 4 \text{ M}_\odot$  the HBB is efficient so that the  $^{13}\text{C}$  overabundance exceeds the  $^{12}\text{C}$  overabundance by about a factor of 10. Both low-mass stars as well as massive stars produce carbon with much larger isotopic ratio than this (Woosley et al. 2002). A nuclear production site like these intermediate mass stars with a small  $^{12}\text{C}/^{13}\text{C}$  ratio is therefore needed to account for example for the solar ratio of  $^{12}\text{C}/^{13}\text{C} \simeq 89$ .

**Nitrogen** The LCs maintain their isotopic nitrogen enrichment from the first and second DUP. The nitrogen overabundance in these heavily C-enriched model stars is therefore of secondary origin. The upper limit of the nitrogen abundance which can be expected in stars polluted by the LCs is given by the initial metallicity.

Large primary production of  $^{14}\text{N}$  are resulting from combined efficient DUP and HBB for the HCs only. The 5 and  $6 \text{ M}_\odot$  models even show a small  $^{15}\text{N}$  enrichment. The  $^{14}\text{N}/^{15}\text{N}$  ratio is determined by the CN cycle equilibrium value. If DUP and HBB are efficient then the  $^{14}\text{N}$  overproduction is so large that some primary  $^{15}\text{N}$  is produced as well. However, this does not address the problem of the nuclear production site of the solar  $^{15}\text{N}$  abundance. In the absence of detailed models earlier studies have speculated that  $^{15}\text{N}$  may be produced in IMS (Timmes et al. 1995). This possibility can be ruled out at least for models which employ rather standard physical assumptions.

Finally note that the carbon to nitrogen ratio in the ejecta of IMS stars is almost bimodal. The LCs have large [C/N] while the HCs have small ratios. With standard assumptions on mixing the mass transition between high and low [C/N] is very sharp. It is therefore not clear that the simultaneous C and N enrichment observed in many EMP CH-stars can be explained by mass transfer from companion stars that have evolved like any of the models presented here.

**Oxygen**  $^{16}\text{O}$  is enhanced in the envelopes of EMP AGB stars by third dredge-up. The pattern is the same as in the case  $^{12}\text{C}$ : the lower mass cases bring cumulatively more intershell material into the envelope compared to the higher mass cases. The origin of  $^{16}\text{O}$  is the  $^{12}\text{C}(\alpha, \gamma)^{16}\text{O}$  reaction transforming primary  $^{12}\text{C}$  from the triple- $\alpha$  reaction.  $^{16}\text{O}$  is mainly produced in the lower part of the He-shell where the  $^4\text{He}$  abundance is declining. During the He-shell flash the triple- $\alpha$  reaction dominates. The amount of  $^{16}\text{O}$  available in the convectively mixed intershell depends on the treatment of convective boundaries. With our assumption of exponential overshoot at the bottom of the PDCZ an  $^{16}\text{O}$  abundance in this layer of about 6% by mass is found, depending somewhat on TP number and mass. As shown

in Paper I the prediction of significant dredge-up of  $^{16}\text{O}$  in EMP AGB stars is not a result of assuming overshooting at the bottom of the PDCZ. Even without this kind of extra-mixing the  $^{16}\text{O}$  abundance in the PDCZ in EMP stars is of the order 1 – 2% by mass. This primary oxygen in the intershell is in any case several orders of magnitude more abundant than the initial  $^{16}\text{O}$  abundance in the envelope. The importance of  $^{16}\text{O}$  dredge-up in AGB stars of the lowest AGB stars is also found in the calculation for metallicity  $Z=0$  by Siess et al. (2002). For example at the end of the evolution of their  $1.5\text{ M}_\odot$  model which does not experience HBB the surface  $^{12}\text{C}$ -mass fraction is  $6.9 \cdot 10^{-3}$  and that of  $^{16}\text{O}$  is  $2.4 \cdot 10^{-3}$

The  $^{18}\text{O}$  abundance is depleted rather rapidly for the HCs during HBB and not replenished because the  $^{17}\text{O}(\text{p}, \alpha)^{14}\text{N}$  reaction exceeds the  $^{17}\text{O}(\text{p}, \alpha)^{18}\text{F}$  reaction by almost two orders of magnitude.

**Neon** A small primary production of  $^{20}\text{Ne}$  can be noted for all masses (Fig. 9). This is just a curiosity as the nuclear origin of  $^{20}\text{Ne}$  is carbon burning in supernova Type II. However, it is noted that the small increase of  $^{20}\text{Ne}$  observed in these models is due to two reactions:  $^{16}\text{O}(\alpha, \gamma)^{20}\text{Ne}$  and to a lesser degree  $^{16}\text{O}(\text{n}, \gamma)^{17}\text{O}(\alpha, \text{n})^{20}\text{Ne}$ .

In the LCs the primary  $^{22}\text{Ne}$  can increase the elemental neon abundance significantly. Both heavy neon isotopes are destroyed by HBB in the HC cases. During the final pulse cycles HBB becomes less efficient. Only then is the DUP of  $^{21}\text{Ne}$  and  $^{22}\text{Ne}$  more efficient than the interpulse destruction. In the He-shell flash  $^{21}\text{Ne}$  is mainly made by  $^{16}\text{O}(\text{n}, \gamma)^{17}\text{O}(\alpha, \gamma)^{21}\text{Ne}$  and to a small extent by  $^{20}\text{Ne}(\text{n}, \gamma)^{21}\text{Ne}$ . In the LCs in particular the  $^{21}\text{Ne}$  yields are significant. It is important to note that even if the  $^{20}\text{Ne}(\text{n}, \gamma)^{21}\text{Ne}$  dominates  $^{21}\text{Ne}$  is still primary, because  $^{20}\text{Ne}$  is produced in a primary mode, even though this is not important for the  $^{22}\text{Ne}$  yield at this metallicity.

**Sodium** Sodium is produced by both LCs and HCs by different processes. In HCs  $^{22}\text{Ne}$  is dredged up from the intershell and then transformed into  $^{23}\text{Na}$  during HBB. If, like in the  $6\text{ M}_\odot$  case, HBB is very efficient then  $^{23}\text{Na}$  is first produced and destroyed in the second half of the interpulse phase. However in all other cases significant amounts of  $^{23}\text{Na}$  are produced. In the LCs the main source of  $^{23}\text{Na}$  is  $^{22}\text{Ne}(\text{n}, \gamma)^{23}\text{Na}$ .

**Magnesium** The different nuclear production sites during H- and He-shell burning in TP-AGB stars is discussed in all detail in Karakas & Lattanzio (2003). Although they have computed models for somewhat higher metallicity all their basic mechanisms apply equally here.  $^{24}\text{Mg}$  is only significantly changed if HBB is very efficient, like in the E0086,  $6\text{ M}_\odot$

case (Fig. 10). Then both  $^{25}\text{Mg}$  as well as  $^{26}\text{Mg}$  are produced. This production mode of the neutron heavy isotopes of magnesium has a distinct signature: the  $^{25}\text{Mg}$  abundance is larger than the  $^{26}\text{Mg}$  abundance (Karakas & Lattanzio 2003; Denissenkov & Herwig 2003). Even taking into account nuclear reaction rate uncertainties does not change this finding.

There is a second production site for the neutron heavy magnesium isotopes. In the He-shell flash convection zone the two  $\alpha$ -captures on  $^{22}\text{Ne}$  are almost equally important:  $^{22}\text{Ne}(\alpha, n)^{25}\text{Mg}$  and  $^{22}\text{Ne}(\alpha, \gamma)^{26}\text{Mg}$ . However, the temperature dependence of these two reactions is different. For  $T_8 > 2.8$  the  $(\alpha, n)$  reaction exceeds the  $(\alpha, \gamma)$  reaction, while for lower temperatures  $^{22}\text{Ne}$  is more effectively transformed into  $^{26}\text{Mg}$ . This dividing temperature coincides roughly with the activation temperature of the  $^{22}\text{Ne}$  n-source reaction. Therefore, for low temperatures in the He-shell flash convection zone (as can be found in low mass models) one expects only little neutron-heavy magnesium production favoring  $^{26}\text{Mg}$ . However, at higher He-shell flash temperatures should  $^{25}\text{Mg}$  dominate the heavy Mg isotope production.

There is a component missing in this picture, which appears to be important in EMP stars.  $^{25}\text{Mg}$  has a very high neutron cross section, about 600 times larger than that of  $^{12}\text{C}$ , about 200 times larger than  $^{16}\text{O}$ , and still about twice as large as the  $^{26}\text{Al}$  n-capture cross section. The relative number of neutrons actually available for  $^{25}\text{Mg}$  depends not only on the relative value of the cross sections but equally on the abundance of competing neutron capturing species. Assuming, for example, that 5% by mass of a 2% mass abundance of  $^{22}\text{Ne}$  is transformed into  $^{25}\text{Mg}$  implies a mass abundance for this isotope of  $10^{-3}$ . Thus, for this example ( $\langle \sigma v \rangle_{(n, \gamma)} Y$ ) $^{25}\text{Mg}$  exceeds ( $\langle \sigma v \rangle_{(n, \gamma)} Y$ ) $^{12}\text{C}$ . Thus, neutrons are captured by  $^{25}\text{Mg}$  in significant numbers if  $^{22}\text{Ne}$  releases neutrons. In order to check this picture I have conducted some one-zone nuclear network calculations for typical conditions found in the He-shell flash convection zone. These calculations confirm that neutron captures on  $^{25}\text{Mg}$  are important for the evolution of the heavy magnesium isotopes in EMP AGB stars. For temperatures where  $^{22}\text{Ne}$  releases neutrons (in the test calculations  $T_8 = 3.2$ )  $X(^{26}\text{Mg}) > X(^{25}\text{Mg})$  if all neutron capture reactions are considered, but  $X(^{26}\text{Mg}) < X(^{25}\text{Mg})$  if the  $^{25}\text{Mg}(n, \gamma)^{26}\text{Mg}$  reaction is switched off, as expected from the ratio of two  $^{22}\text{Ne}$   $\alpha$  captures.

It should also be pointed out that this  $^{25}\text{Mg}$  and  $^{26}\text{Mg}$  from the He-shell is of primary origin while  $^{25}\text{Mg}$  and  $^{26}\text{Mg}$  from HBB is mainly secondary. There it is produced at the expense of the initial  $^{24}\text{Mg}$  abundance, that has its primary origin during carbon and subsequent neon burning in Type II supernova.

These models show that in fact EMP AGB stars can – within the uncertainties of mass loss in particular – produce primary neutron heavy magnesium isotopes with a  $^{26}\text{Mg}/^{25}\text{Mg}$  ratio exceeding unity. This is in particular the case when mass loss is efficient and prevents

HBB from dominating the nucleosynthesis of the neutron-heavy Mg isotopes. This result should be relevant for the interpretation of recent isotopic magnesium abundance determinations (Yong et al. 2003).

**More comparison with other calculations** Ventura et al. (2002) have presented IMS yields from complete stellar evolution calculations down to a metallicity of  $Z=0.0002$ . They focus on the evolution of helium and the CNO elements and have not included any heavier elements. Some of their input physics assumptions are different than those adopted in this study. These include in particular their choices on the treatment of convection. They use the Full-Spectrum Turbulence theory (Canuto & Mazzitelli 1991) which tends to cause more efficient HBB compared to the standard MLT. More importantly, they chose to apply no overshooting or any other means of extra-mixing during the TP-AGB phase. Even at very low metallicities and the corresponding high core masses their third dredge-up is as small as  $\lambda = 0.2 \dots 0.4$ . As a result their average masses in the ejected material of species like  ${}^4\text{He}$ ,  ${}^{12}\text{C}$  or  ${}^{16}\text{O}$  are significantly smaller than in this study (Fig. 11). A probably small part of this difference may be attributed to the metallicity difference of a factor of two between the two sets. However, while the two sets of models are quantitatively different the abundance trends with mass are the same.

#### 4. Conclusion

This paper describes the properties of a grid of intermediate mass stellar evolution models with low metallicity ( $Z=0.0001$ ). The computations include an extensive nuclear reaction network which allow predictions of yields and surface abundance evolution for a large number of species. The model also includes neutron capture reactions which appear to be important for the correct modeling of light neutron heavy isotopes. A rather small amount of exponential overshooting has been included. No other non-standard effects (like rotation or magnetic fields) have been considered. Thus, these are rather standard models with updated input physics.

Confronting models and observations at very low metallicity is especially interesting as Galactic Chemical Evolution had less time to cover the tracks of individual nuclear production events. In this lies the importance of studying stars of the lowest metallicity, both theoretically and observationally. Confronting these standard models with observations of EMP stars will help to identify what additional processes are important.

The amount of exponential overshoot in these models is too small to generate a  ${}^{13}\text{C}$

pocket that could create relevant neutron fluxes. However, the yields of some neutron-heavy isotopes have been shown in this paper to be very sensitive to the s-process in EMP stars. In these models the neutrons come almost exclusively from the He-shell flash convection zone and  $^{22}\text{Ne}$  as the neutron source. In the future the role of the  $^{13}\text{C}$  pocket for the s-process in general and for the EMP yields of species like the heavy magnesium isotopes must be studied in more detail.

F. H. appreciates generous support from D. A. VandenBerg through his Operating Grant from the Natural Science and Engineering Research Council of Canada. This work would have not been possible without our stellar evolution computer cluster. I would also like to thank Maria Lugardo for many important discussions on the s-process.

## REFERENCES

Angulo, C., Arnould, M., & Rayet, M. et al. 1999, Nucl. Phys., A 656, 3, NACRE compilation

Bao, Z. Y., Beer, H., Käppeler, F., Voss, F., Wissak, K., & Rauscher, T. 2000a, ADNDT, 76, 70

—. 2000b, ADNDT, 75, 1

Beer, H., Sedyshev, P., Rochow, W., & Oberhummer, P. M. H. 2001, Nucl. Phys. A, 705, 239

Blöcker, T. 1993, PhD thesis, Universität Kiel, Germany

—. 1995, A&A, 297, 727

Bowen, G. H. 1988, ApJ, 329, 299

Canuto, V. M. & Mazzitelli, I. 1991, ApJ, 370, 295

Caughlan, G. R. & Fowler, W. A. 1988, Atom. Data Nucl. Data Tables, 40, 283, cF88

Chieffi, A., Dominguez, I., Limongi, M., & Straniero, O. 2001, ApJ, 554, 1159

Denissenkov, P. A. & Herwig, F. 2003, ApJ Lett., 590, L99

Dreizler, S., Werner, K., Heber, U., & Engels, D. 1996, A&A, 309, 820

Girardi, L., Bressan, A., Chiosi, C., Bertelli, G., & Nasi, E. 1996, A&AS, 117, 113

Goriely, S. 1999, A&A, 342, 881

Goriely, S. & Mowlavi, N. 2000, A&A, 362, 599

Herwig, F. 2000, A&A, 360, 952

—. 2004, ApJ, 605, 425

Herwig, F. & Austin, S. M. 2004, ApJ Lett., submitted

Herwig, F., Blöcker, T., Schönberner, D., & El Eid, M. F. 1997, A&A, 324, L81

Herwig, F., Langer, N., & Lugaro, M. 2003, ApJ, 593, 1056

Horiguchi, T., Tachibana, T., & Katakura, J. 1996, in Chart of the Nuclides (Japanese Nuclear Data Committee and Nuclear Data Center; Japan Atomic Energy Research Institute)

Iliadis, C., D'Auria, J. M., Starrfield, S., Thompson, W. J., & Wiescher, M. 2001, ApJS, 134, 151

Jorissen, A. & Goriely, S. 2001, Nucl. Phys., A 688, 508, nETGEN database

Karakas, A. I. & Lattanzio, J. C. 2003, PASA, 20, 279

Karakas, A. I., Lattanzio, J. C., & Pols, O. R. 2002, PASA, 19, 515

Koehler & O'Brien. 1989, Phys. Rev. C., 39, 1655

Koesterke, L. & Hamann, W. R. 1997, A&A, 320, 91

Langer, N., Heger, A., Wellstein, S., & Herwig, F. 1999, A&A, 346, L37

Lugaro, M., Herwig, F., Lattanzio, J. C., Gallino, R., & Straniero, O. 2003, ApJ, 586, 1305

Marigo, P. 1998, A&A, 340, 463

—. 2002, A&A, 387, 507

Marigo, P., Bressan, A., & Chiosi, C. 1996, A&A, 313, 545

Marigo, P., Girardi, L., & Bressan, A. 1999, A&A, 344, 123

Mowlavi, N. 1999, A&A, 344, 617

Pettini, M., Ellison, S. L., Bergeron, J., & Petitjean, P. 2002, A&A, 391, 21

Renzini, A. & Voli, M. 1981, A&A, 94, 175

Siess, L., Livio, M., & Lattanzio, J. 2002, ApJ, 570, 329

Takahashi, K. & Yokoi, K. 1987, ADNDT, 36, 375

Timmes, F. X., Woosley, S. E., & Taam, R. E. 1994, ApJ, 420, 348

Timmes, F. X., Woosley, S. E., & Weaver, T. A. 1995, APJS, 98, 617

van den Hoek, L. & Groenewegen, M. 1997, A&AS, 123, 305

van Loon, J. T. 2000, A&A, 354, 125

Ventura, P., D'Antona, F., & Mazzitelli, I. 2002, A&A, 393, 215

Walker, T. P., Steigman, G., Kang, H., Schramm, D. M., & Olive, K. A. 1991, ApJ, 376, 51

Werner, K. & Herwig, F. 2005, PASP, 000, 000, in prep

Wiescher, M., Goerres, J., & Thielemann, F.-K. 1990, ApJ, 363, 340

Woosley, S. E., Heger, A., & Weaver, T. A. 2002, Rev. Mod. Phys., 74, 1015

Yong, D., Grundahl, F., Lambert, D. L., Nissen, P. E., & Shetrone, M. D. 2003, A&A, 402, 985

Zijlstra, A. A. 2004, MNRAS, 348, L23

Table 1. Reaction network EDITOR: this table electronically only

ID	Reaction			Ref.	
p-capture reactions					
1	2 PROT	( 0 00000, 0 00000)	1 DEUT	1	
2	1 DEUT	( 1 PROT , 0 00000)	1 HE 3	1	
6	1 LI 7	( 1 PROT , 0 00000)	2 HE 4	1	
7	1 BE 7	( 1 PROT , 0 00000)	1 B 8	1	
10	1 C 12	( 1 PROT , 0 00000)	1 N 13	1	
11	1 C 13	( 1 PROT , 0 00000)	1 N 14	1	
12	1 N 14	( 1 PROT , 0 00000)	1 O 15	1	
13	1 N 15	( 1 PROT , 1 HE 4)	1 C 12	1	
14	1 N 15	( 1 PROT , 0 00000)	1 O 16	1	
15	1 O 16	( 1 PROT , 0 00000)	1 F 17	1	
16	1 O 17	( 1 PROT , 1 HE 4)	1 N 14	1	
17	1 O 17	( 1 PROT , 0 00000)	1 F 18	1	
18	1 O 18	( 1 PROT , 1 HE 4)	1 N 15	1	
19	1 O 18	( 1 PROT , 0 00000)	1 F 19	1	
20	1 F 19	( 1 PROT , 1 HE 4)	1 O 16	1	
21	1 F 19	( 1 PROT , 0 00000)	1 NE 20	1	
22	1 NE 20	( 1 PROT , 0 00000)	1 NA 21	1	
23	1 NE 21	( 1 PROT , 0 00000)	1 NA 22	1	
26	1 NA 22	( 1 PROT , 0 00000)	1 MG 23	1	
30	1 MG 25	( 1 PROT , 0 00000)	1 AL 26g	1	
33	1 AL 26g	( 1 PROT , 0 00000)	1 SI 27	4	
35	1 AL 27	( 1 PROT , 1 HE 4)	1 MG 24	1	
37	1 SI 28	( 1 PROT , 0 00000)	1 P 29	1	
38	1 SI 29	( 1 PROT , 0 00000)	1 P 30	1	
39	1 SI 30	( 1 PROT , 0 00000)	1 P 31	1	
63	1 NE 22	( 1 PROT , 0 00000)	1 NA 23	1	
65	1 NA 23	( 1 PROT , 0 00000)	1 MG 24	1	
66	1 NA 23	( 1 PROT , 1 HE 4)	1 NE 20	1	

Table 1—Continued

ID	Reaction	Ref.
69	1 MG 24 ( 1 PROT , 0 00000)	1 AL 25 1
70	1 MG 25 ( 1 PROT , 0 00000)	1 AL 26 1
72	1 MG 26 ( 1 PROT , 0 00000)	1 AL 27 1
73	1 AL 27 ( 1 PROT , 0 00000)	1 SI 28 1
74	1 AL 27 ( 1 PROT , 1 HE 4)	1 MG 24 1
79	1 B 11 ( 1 PROT , 0 00000)	3 HE 4 1
81	1 C 14 ( 1 PROT , 0 00000)	1 N 15 a
92	1 N 13 ( 1 PROT , 0 00000)	1 O 14 1
101	1 P 31 ( 1 PROT , 0 00000)	1 S 32 4
$\alpha$ - and $^3\text{He}$ -capture reactions		
3	2 HE 3 ( 0 00000, 2 PROT )	1 HE 4 1
4	1 HE 4 ( 1 HE 3, 0 00000)	1 BE 7 1
40	3 HE 4 ( 0 00000, 0 00000)	1 C 12 1
41	1 C 12 ( 1 HE 4, 0 00000)	1 O 16 1
42	1 C 13 ( 1 HE 4, 1 NEUT )	1 O 16 1
43	1 N 14 ( 1 HE 4, 0 00000)	1 F 18 1
44	1 O 16 ( 1 HE 4, 0 00000)	1 NE 20 1
45	1 O 18 ( 1 HE 4, 0 00000)	1 NE 22 1
46	1 NE 20 ( 1 HE 4, 0 00000)	1 MG 24 1
48	1 NE 21 ( 1 HE 4, 1 NEUT )	1 MG 24 1
49	1 NE 22 ( 1 HE 4, 0 00000)	1 MG 26 1
50	1 NE 22 ( 1 HE 4, 1 NEUT )	1 MG 25 1
53	1 MG 24 ( 1 HE 4, 0 00000)	1 SI 28 3
61	1 NE 20 ( 1 HE 4, 1 PROT )	1 NA 23 1
67	1 NA 23 ( 1 HE 4, 1 PROT )	1 MG 26 8
68	1 MG 24 ( 1 HE 4, 1 PROT )	1 AL 27 1
71	1 MG 25 ( 1 HE 4, 1 NEUT )	1 SI 28 1
75	1 BE 7 ( 1 HE 4, 0 00000)	1 C 11 1
76	1 LI 7 ( 1 HE 4, 0 00000)	1 B 11 1

Table 1—Continued

ID	Reaction						Ref.
78	1 B 11	( 1 HE 4,	1 NEUT )	1 N	14	3	
80	1 C 14	( 1 HE 4,	0 00000)	1 O	18	9	
82	1 N 15	( 1 HE 4,	0 00000)	1 F	19	1	
83	1 O 17	( 1 HE 4,	0 00000)	1 NE 21	3		
84	1 O 17	( 1 HE 4,	1 NEUT )	1 NE 20	1		
n-capture reactions							
31	1 AL 26g	( 1 NEUT ,	1 PROT )	1 MG 26	3		
32	1 AL 26g	( 1 NEUT ,	1 HE 4)	1 NA 23	3		
36	1 BE 7	( 1 NEUT ,	1 PROT )	1 LI 7	0		
47	1 NE 20	( 1 NEUT ,	0 00000)	1 NE 21	5		
51	1 NE 22	( 1 NEUT ,	0 00000)	1 NA 23	6		
52	1 NA 23	( 1 NEUT ,	0 00000)	1 MG 24	5		
54	1 MG 24	( 1 NEUT ,	0 00000)	1 MG 25	5		
55	1 MG 25	( 1 NEUT ,	0 00000)	1 MG 26	5		
56	1 MG 26	( 1 NEUT ,	0 00000)	1 AL 27	5		
57	1 AL 27	( 1 NEUT ,	0 00000)	1 SI 28	5		
58	1 C 12	( 1 NEUT ,	0 00000)	1 C 13	5		
62	1 NE 21	( 1 NEUT ,	0 00000)	1 NE 22	7		
64	1 NE 22	( 1 NEUT ,	0 00000)	1 NA 23	6		
85	1 N 14	( 1 NEUT ,	1 PROT )	1 C 14	b		
86	1 SI 28	( 1 NEUT ,	0 00000)	1 SI 29	5		
87	1 SI 29	( 1 NEUT ,	0 00000)	1 SI 30	5		
88	1 SI 30	( 1 NEUT ,	0 00000)	1 P 31	5		
89	1 N 14	( 1 NEUT ,	0 00000)	1 N 15	5		
90	1 O 16	( 1 NEUT ,	0 00000)	1 O 17	5		
93	1 FE 56	( 1 NEUT ,	0 00000)	1 FE 57	5		
94	1 FE 57	( 1 NEUT ,	0 00000)	1 FE 58	5		
95	1 FE 58	( 1 NEUT ,	0 00000)	1 CO 59	5		
96	1 CO 59	( 1 NEUT ,	0 00000)	1 NI 60	5		

Table 1—Continued

ID	Reaction	Ref.
97	1 NI 60 ( 1 NEUT , 0 00000)	1 NI 61 5
98	1 NI 61 ( 1 NEUT , 0 00000)	1 NI 62 5
100	1 P 31 ( 1 NEUT , 0 00000)	1 S 32 5
106	1 NI 58 ( 1 NEUT , 0 00000)	1 NI 59 5
107	1 NI 59 ( 1 NEUT , 0 00000)	1 NI 60 e
108	1 NI 59 ( 1 NEUT , 1 PROT )	1 CO 59 8
$\beta$ -decay and $e^-$ -captures		
5	1 BE 7 ( 0 00000, 0 00000)	1 LI 7 1
8	1 B 8 ( 0 00000, 0 00000)	2 HE 4 1
9	1 B 8 ( 0 00000, 1 PROT )	1 BE 7 1
25	1 NA 22 ( 0 00000, 0 00000)	1 NE 22 2
34	1 AL 26g( 0 00000, 0 00000)	1 MG 26 2
77	1 C 11 ( 0 00000, 0 00000)	1 B 11 2
91	1 N 13 ( 0 00000, 0 00000)	1 C 13 2
104	1 C 14 ( 0 00000, 0 00000)	1 N 14 c
105	1 NI 59 ( 0 00000, 0 00000)	1 CO 59 d
C-burning		
59	2 C 12 ( 0 00000, 1 PROT )	1 NA 23 3
60	2 C 12 ( 0 00000, 1 HE 4)	1 NE 20 3

1: NACRE adopted; 2: Horiguchi et al. (1996); 3: Caughlan & Fowler (1988); 4: Iliadis et al. (2001); 5: Bao et al. (2000a); 6: Beer et al. (2001); 7: Bao et al. (2000b); 8: Hauser-Feshbach (Jorissen & Goriely 2001); 9: see Jorissen & Goriely (2001); a: Wiescher et al. (1990); b: Koehler & O’Brien (1989); c: Takahashi & Yokoi (1987); d: Goriely (1999); e: Hauser-Feshbach (Jorissen & Goriely 2001)

Table 2. Model properties I

ID	$M_{\text{ini}}$ $M_{\odot}$	$m_{\text{c}}^a$ $m_{\text{c}}$	$\log L_{\star}^b$ $L_{\odot}$	$R_{\star}^b$ $R_{\odot}$	$N_{\text{TD}}^c$ $N_{\text{TD}}$	$t_{\text{TP1}}^d$ $10^6 \text{ yr}$	$\Delta M_{\text{Dmax}}^e$ $10^{-2} M_{\odot}$	$M_{\text{D}}^f$ $10^{-2} M_{\odot}$	$t_{\text{ip}}^g$ $\text{yr}$	$M_{\text{lost}}^h$ $M_{\odot}$
E82	2	$0.626 \pm 0.006$	3.96	180	6	799.1	1.171	5.038	82731	1.34
E84	3	$0.814 \pm 0.006$	4.25	250	9	277.1	0.507	3.465	14116	2.13
E85	4	$0.887 \pm 0.002$	4.40	300	10	151.0	0.367	2.707	8457	3.05
E79	5	$0.947 \pm 0.001$	4.63	360	12	97.2	0.308	2.422	5281	3.99
E86	6	$1.033 \pm 0.001$	4.70	420	15	68.6	0.140	1.241	2416	4.83

<sup>a</sup>mass of H-free core, range gives total range of core mass evolution, <sup>b</sup>approximate average

for the entire sequence, <sup>c</sup>number of TPs with DUP, <sup>d</sup> time at first TP, <sup>e</sup> maximum dredged-up mass after a single TP, <sup>f</sup> total dredged-up mass all TPs, <sup>g</sup> average interpulse duration of TPs with DUP, <sup>h</sup> total mass lost= $M_{\star}$  at first TP minus  $m_{\text{HTP}}$  at end of AGB.

Table 3. Model properties II

TP	$t_{\text{TP}}^a$	$T_{\text{FBOT}}^b$	$T_{\text{HES}}^c$	$T_{\text{HS}}^d$	$T_{\text{CEB}}^e$	$m_{\text{FBOT}}^f$	$m_{\text{HTP}}^g$	$m_{\text{DMAX}}^h$	$M_{\star}^i$
E82, $M=2 M_{\odot}$									
1	$3.97E - 02$	8.32	8.10	7.83	6.31	0.60550	0.62559	0.62740	1.97251
2	$8.23E + 04$	8.42	8.09	7.81	6.48	0.60264	0.62884	0.62524	1.96576
3	$1.74E + 05$	8.44	7.93	7.80	6.65	0.60278	0.63041	0.62403	1.93878
4	$2.70E + 05$	8.46	7.92	7.80	6.74	0.60424	0.63132	0.62279	1.86456
5	$3.71E + 05$	8.48	7.93	7.79	6.79	0.60230	0.63193	0.62088	1.70939
6	$4.76E + 05$	8.49	7.93	7.79	6.70	0.60210	0.63144	0.61973	1.44626
7	$5.79E + 05$	8.50	7.94	7.78	6.20	0.60065	0.63111	0.62021	1.00773
End of AGB						0.62768			0.62823
E84, $M=3 M_{\odot}$									
1	$2.05E - 04$	8.38	8.16	7.91	6.70	0.81151	0.81896	0.81825	2.94292
2	$1.13E + 04$	8.43	8.14	7.90	6.99	0.81156	0.81945	0.81711	2.92614
3	$2.40E + 04$	8.46	7.98	7.89	7.19	0.81103	0.81898	0.81573	2.88628
4	$3.86E + 04$	8.48	7.99	7.88	7.34	0.81034	0.81819	0.81430	2.81285
5	$5.46E + 04$	8.50	8.00	7.88	7.47	0.80858	0.81726	0.81274	2.68487
6	$7.17E + 04$	8.51	8.01	7.88	7.56	0.80752	0.81618	0.81129	2.50025
7	$8.94E + 04$	8.52	8.01	7.88	7.57	0.80644	0.81508	0.81011	2.23381
8	$1.08E + 05$	8.53	8.08	7.88	7.41	0.80549	0.81414	0.80907	1.87774
9	$1.27E + 05$	8.54	8.08	7.87	6.49	0.80465	0.81331	0.80830	1.40821
End of AGB						0.81251			0.81343
E85, $M=4 M_{\odot}$									
1	$0.00E + 00$	8.47	8.35	7.93	7.72	0.88627	0.89069	0.88702	3.93490
2	$1.19E + 04$	8.48	8.34	7.94	7.82	0.88628	0.89012	0.88756	3.81435
3	$2.01E + 04$	8.50	8.36	7.94	7.87	0.88570	0.88974	0.88648	3.65361

Table 3—Continued

TP	$t_{\text{TP}}^a$	$T_{\text{FBOT}}^b$	$T_{\text{HES}}^c$	$T_{\text{HS}}^d$	$T_{\text{CEB}}^e$	$m_{\text{FBOT}}^f$	$m_{\text{HTP}}^g$	$m_{\text{DMAX}}^h$	$M_{\star}^i$
4	$3.00E + 04$	8.50	8.06	7.94	7.89	0.88547	0.88926	0.88611	3.36429
5	$3.98E + 04$	8.52	8.06	7.94	7.89	0.88511	0.88888	0.88563	3.00263
6	$4.98E + 04$	8.53	8.06	7.94	7.87	0.88478	0.88847	0.88566	2.55257
7	$5.85E + 04$	8.54	8.07	7.93	7.81	0.88428	0.88824	0.88518	2.12662
8	$6.73E + 04$	8.55	8.08	7.92	7.58	0.88380	0.88785	0.88481	1.72477
9	$7.62E + 04$	8.55	8.11	7.91	6.42	0.88337	0.88752	0.88621	1.36279
10	$8.44E + 04$	8.55	8.00	7.90	5.23	0.88469	0.88843	0.88747	0.98297
End of AGB							0.88783		0.88916
E79, M=5 M <sub>⊙</sub>									
1	$-8.10E + 01$	8.36	8.20	7.99	7.38	0.94796	0.95020	0.95024	4.93359
2	$2.64E + 03$	8.40	8.18	7.99	7.50	0.94837	0.95075	0.95013	4.91927
3	$5.32E + 03$	8.44	8.08	7.97	7.96	0.94819	0.95083	0.94774	4.90782
4	$1.22E + 04$	8.48	8.09	7.98	7.94	0.94727	0.94991	0.94701	4.79325
5	$1.92E + 04$	8.50	8.10	7.98	7.89	0.94655	0.94907	0.94645	4.56126
6	$2.64E + 04$	8.51	8.10	7.98	7.96	0.94605	0.94843	0.94597	4.13737
7	$3.35E + 04$	8.52	8.10	7.98	7.95	0.94558	0.94795	0.94560	3.54257
8	$4.02E + 04$	8.52	8.10	7.98	7.94	0.94529	0.94754	0.94555	2.90971
9	$4.62E + 04$	8.53	8.10	7.97	7.92	0.94510	0.94740	0.94550	2.38893
10	$5.14E + 04$	8.54	8.11	7.96	7.86	0.94494	0.94730	0.94547	2.01317
11	$5.61E + 04$	8.55	8.11	7.95	7.71	0.94468	0.94723	0.94531	1.72970
12	$6.10E + 04$	8.56	8.12	7.94	7.35	0.94440	0.94706	0.94524	1.49238
13	$6.58E + 04$	8.56	8.13	7.94	5.96	0.94431	0.94691	0.94614	1.25506
14	$7.03E + 04$	8.56	—	—	—	0.94486	0.94756	—	1.01774
End of AGB							0.94496		0.94613
E86, M=6 M <sub>⊙</sub>									
1	$-2.29E - 01$	8.37	8.22	8.03	7.92	1.03266	1.03362	1.03365	5.86578

Table 3—Continued

TP	$t_{\text{TP}}^a$	$T_{\text{FBOT}}^b$	$T_{\text{HES}}^c$	$T_{\text{HS}}^d$	$T_{\text{CEB}}^e$	$m_{\text{FBOT}}^f$	$m_{\text{HTP}}^g$	$m_{\text{DMAX}}^h$	$M_{\star}^i$
2	$1.05E + 03$	8.39	8.21	8.04	7.96	1.03297	1.03397	1.03391	5.85307
3	$2.11E + 03$	8.41	8.21	8.05	7.98	1.03323	1.03426	1.03414	5.83891
4	$3.17E + 03$	8.43	8.14	8.05	8.00	1.03348	1.03450	1.03323	5.82221
5	$6.54E + 03$	8.45	8.13	8.05	8.02	1.03327	1.03424	1.03306	5.59171
6	$1.00E + 04$	8.49	8.11	8.05	8.03	1.03290	1.03403	1.03263	5.16970
7	$1.36E + 04$	8.50	8.12	8.04	8.03	1.03255	1.03358	1.03246	4.45788
8	$1.70E + 04$	8.53	8.12	8.04	8.02	1.03226	1.03340	1.03236	3.74248
9	$1.99E + 04$	8.53	8.11	8.03	8.02	1.03215	1.03328	1.03226	3.15401
10	$2.25E + 04$	8.54	8.12	8.02	8.00	1.03201	1.03319	1.03229	2.64631
11	$2.50E + 04$	8.54	8.12	8.02	7.97	1.03201	1.03311	1.03221	2.33477
12	$2.72E + 04$	8.55	8.12	8.01	7.94	1.03192	1.03312	1.03221	2.09245
13	$2.92E + 04$	8.55	8.12	8.00	7.90	1.03189	1.03309	1.03222	1.88476
14	$3.12E + 04$	8.56	8.13	7.99	7.79	1.03186	1.03311	1.03227	1.71168
15	$3.32E + 04$	8.57	8.16	7.98	7.63	1.03180	1.03312	1.03281	1.56168
16	$3.50E + 04$	8.57	8.16	7.98	7.29	1.03222	1.03354	1.03327	1.45783
17	$3.69E + 04$	8.57	—	—	6.20	1.03272	1.03402	1.03377	1.29629
End of AGB						1.034962			1.065924

<sup>a</sup> time since first TP,  $t = 0$  yr at about the time of the He-luminosity maximum during the first TP; <sup>b</sup> Largest temperature at the bottom of the flash-convection zone; <sup>c</sup> Temperature

in the He-burning shell during the interpulse phase following the thermal pulse; <sup>d</sup>

Temperature in the H-burning shell during the interpulse phase following the TP; <sup>e</sup>

Temperature at the convective envelope bottom during the interpulse phase following the TP; <sup>f</sup> Mass coordinate of the flash-driven convection zone bottom; <sup>g</sup> Mass coordinate of

the H-free core at the time of the TP; <sup>h</sup> Mass coordinate of the convective envelope bottom

at the end of the DUP phase; <sup>i</sup> Stellar mass at the TP.

Table 4. Average mass fractions in material returned to the ISM

No	species	$X_{\text{ini}}$ solar-scaled	E0082 $2 M_{\odot}$	E0084 $3 M_{\odot}$	E0085 $4 M_{\odot}$	E0079 $5 M_{\odot}$	E0086 $6 M_{\odot}$
2	PROT	7.6966E-01	7.260E-01	7.336E-01	6.890E-01	6.600E-01	6.431E-01
5	HE 4	2.3025E-01	2.569E-01	2.588E-01	3.070E-01	3.375E-01	3.558E-01
9	C 12	1.4750E-05	1.369E-02	6.090E-03	8.980E-04	4.587E-04	2.159E-04
10	C 13	1.7750E-07	5.379E-07	6.206E-06	8.565E-05	4.372E-05	3.025E-05
11	N 14	4.5551E-06	2.065E-05	1.742E-05	2.331E-03	1.680E-03	8.002E-04
12	N 15	1.7950E-08	6.114E-09	4.338E-09	6.465E-08	4.431E-08	2.023E-08
13	O 16	4.1401E-05	2.858E-03	1.239E-03	6.110E-04	3.008E-04	1.006E-04
14	O 17	1.6750E-08	7.067E-07	5.453E-07	9.978E-07	8.188E-07	4.392E-07
15	O 18	9.3502E-08	4.984E-08	4.930E-08	1.877E-09	4.783E-10	6.399E-11
17	NE 20	7.6501E-06	1.548E-05	1.837E-05	1.454E-05	1.168E-05	9.676E-06
18	NE 21	1.9500E-08	1.002E-06	9.041E-07	2.460E-07	1.020E-07	3.139E-08
19	NE 22	6.1501E-07	2.733E-04	5.500E-05	1.272E-05	4.035E-06	6.782E-07
21	NA 23	1.6550E-07	3.004E-06	1.737E-06	8.356E-06	3.645E-06	4.964E-07
22	MG 24	2.5250E-06	3.351E-06	2.914E-06	3.016E-06	2.873E-06	2.884E-07
23	MG 25	3.3251E-07	4.961E-06	5.390E-06	3.291E-06	2.825E-06	3.794E-06
24	MG 26	3.8101E-07	6.937E-06	1.155E-05	7.589E-06	4.351E-06	2.657E-06
25	AL26G	1.3000E-26	4.531E-10	6.980E-10	1.109E-08	5.930E-08	3.028E-07
26	AL 27	2.8550E-07	3.639E-07	4.798E-07	4.679E-07	4.608E-07	6.706E-07
27	SI 28	3.2051E-06	3.241E-06	3.323E-06	3.343E-06	3.293E-06	3.423E-06
28	SI 29	1.6800E-07	1.842E-07	1.955E-07	2.035E-07	1.881E-07	1.780E-07
29	SI 30	1.1550E-07	1.244E-07	1.353E-07	1.442E-07	1.320E-07	1.240E-07
47	G 63	1.7000E-08	1.499E-07	8.597E-08	5.737E-08	4.277E-08	3.272E-08
48	L 1	1.0000E-50	1.496E-08	1.799E-08	1.207E-08	6.800E-09	3.551E-09

*a*

Table 5. Yields EDITOR: this table only in the electronic version

No	species	E0082 2 M <sub>⊙</sub>	E0084 3 M <sub>⊙</sub>	E0085 4 M <sub>⊙</sub>	E0079 5 M <sub>⊙</sub>	E0086 6 M <sub>⊙</sub>
2	PROT	-5.955E-02	-7.794E-02	-2.493E-01	-4.335E-01	-6.156E-01
5	HE 4	3.633E-02	6.174E-02	2.372E-01	4.238E-01	6.104E-01
9	C 12	1.867E-02	1.314E-02	2.731E-03	1.754E-03	9.783E-04
10	C 13	4.921E-07	1.304E-05	2.643E-04	1.720E-04	1.462E-04
11	N 14	2.197E-05	2.784E-05	7.193E-03	6.619E-03	3.869E-03
12	N 15	-1.616E-08	-2.945E-08	1.444E-07	1.042E-07	1.111E-08
13	O 16	3.846E-03	2.590E-03	1.761E-03	1.025E-03	2.879E-04
14	O 17	9.421E-07	1.143E-06	3.034E-06	3.169E-06	2.054E-06
15	O 18	-5.962E-08	-9.562E-08	-2.833E-07	-3.676E-07	-4.544E-07
17	NE 20	1.069E-05	2.318E-05	2.131E-05	1.592E-05	9.851E-06
18	NE 21	1.342E-06	1.914E-06	7.005E-07	3.259E-07	5.785E-08
19	NE 22	3.724E-04	1.177E-04	3.744E-05	1.351E-05	3.071E-07
21	NA 23	3.875E-06	3.400E-06	2.532E-05	1.375E-05	1.609E-06
22	MG 24	1.127E-06	8.415E-07	1.519E-06	1.375E-06	-1.088E-05
23	MG 25	6.320E-06	1.094E-05	9.149E-06	9.848E-06	1.683E-05
24	MG 26	8.952E-06	2.417E-05	2.229E-05	1.569E-05	1.107E-05
25	AL26G	6.187E-10	1.510E-09	3.430E-08	2.343E-07	1.473E-06
26	AL 27	1.070E-07	4.202E-07	5.640E-07	6.925E-07	1.873E-06
27	SI 28	4.875E-08	2.542E-07	4.257E-07	3.458E-07	1.058E-06
28	SI 29	2.213E-08	5.959E-08	1.098E-07	7.953E-08	4.866E-08
29	SI 30	1.211E-08	4.288E-08	8.859E-08	6.501E-08	4.115E-08
47	G 63	1.815E-07	1.492E-07	1.248E-07	1.018E-07	7.646E-08
48	L 1	2.043E-08	3.891E-08	3.732E-08	2.687E-08	1.727E-08

*a*

Table 6. Structure and abundance evolution of computed tracks<sup>a</sup>

model	$M_\star$	$t/\text{yr}$	$\log T_{\text{eff}}$	$\log L$	H	${}^4\text{He}$	${}^{12}\text{C}$	...
5029	2.00	$-7.18 \cdot 10^5$	3.67	3.21	$7.56 \cdot 10^{-1}$	$2.44 \cdot 10^{-1}$	$7.12 \cdot 10^{-6}$	...
5814	1.99	$3.23 \cdot 10^2$	3.66	3.48	$7.55 \cdot 10^{-1}$	$2.454 \cdot 10^{-1}$	$7.00 \cdot 10^{-6}$	...
...	...	...	...	...	...	...	...	...

<sup>a</sup> The complete tables ASPS.E82, ASPS.E84, ASPS.E85, ASPS.E79 and ASPS.E86 are available electronically. They contain for each sequence several structural and abundance quantities at 70 - 150 times during the TP-AGB evolution. Specifically these tables contain: model number, stellar mass in  $M_\odot$ , age ( $t = 0$  at first TP),  $\log T_{\text{eff}}$ ,  $\log L / L_\odot$  and the surface abundance evolution of the 23 species given in Table 4. The models in each sequence ahve been selected to reconstruct the abundance evolution. All details of the stellar parameter evolution (for example the exact stellar luminosity evolution after the thermal pulses) are only available from the complete evolution sequence, which can be obtained from the author.

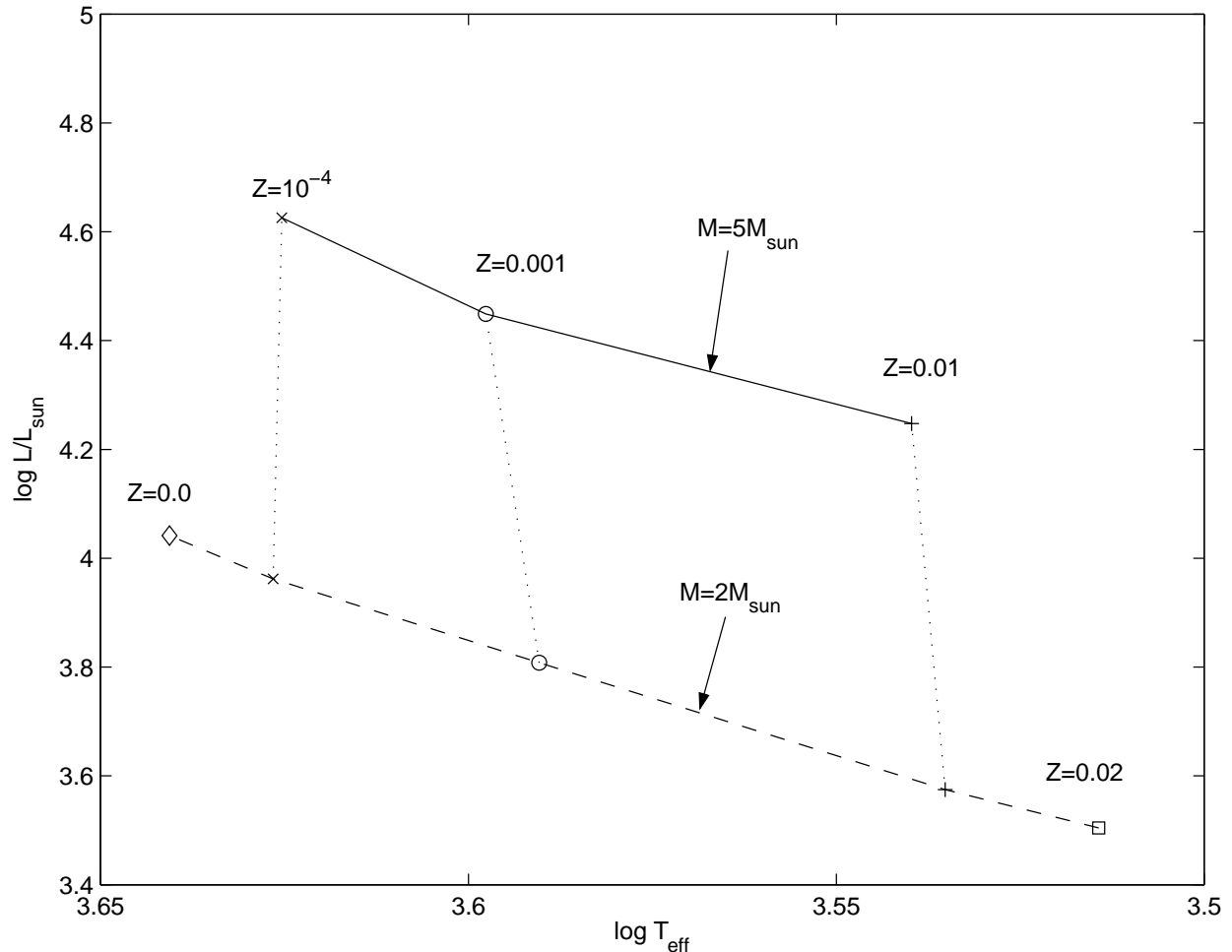


Fig. 1.— Trends of stellar parameters of TP-AGB stellar models for two initial masses and a range of metallicities. The symbols represent values that roughly average the variations of the stellar parameters as a function of the TP cycle as well as the evolution towards the tip of the AGB.

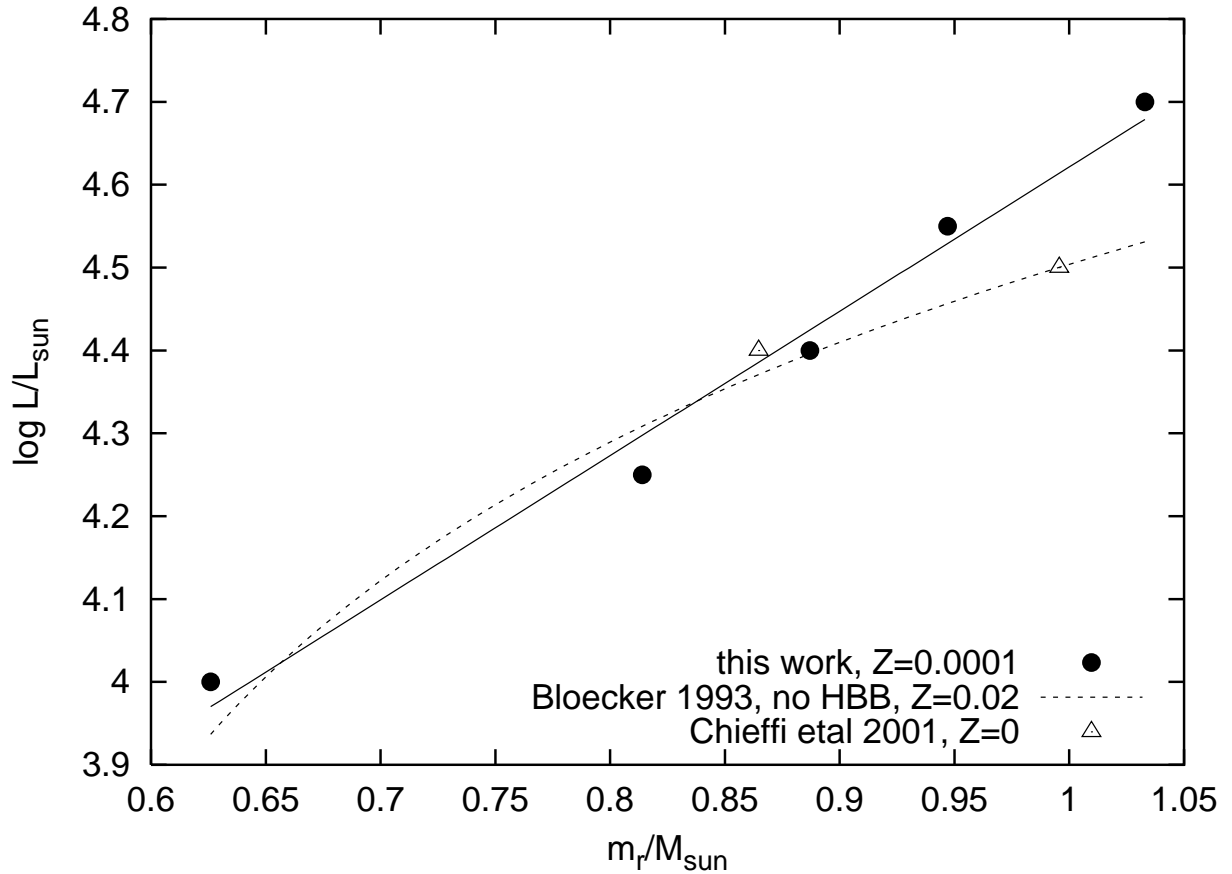


Fig. 2.— Average core masses and stellar luminosities of the 5  $Z=0.0001$  sequences, with a linear  $m_c - \log L$ -fit. As a comparison the core-mass luminosity relation by Blöcker (1993) for non-HBB models and two points for  $Z=0$  TP-AGB models during the last computed interpulse phase by Chieffi et al. (2001) are shown.

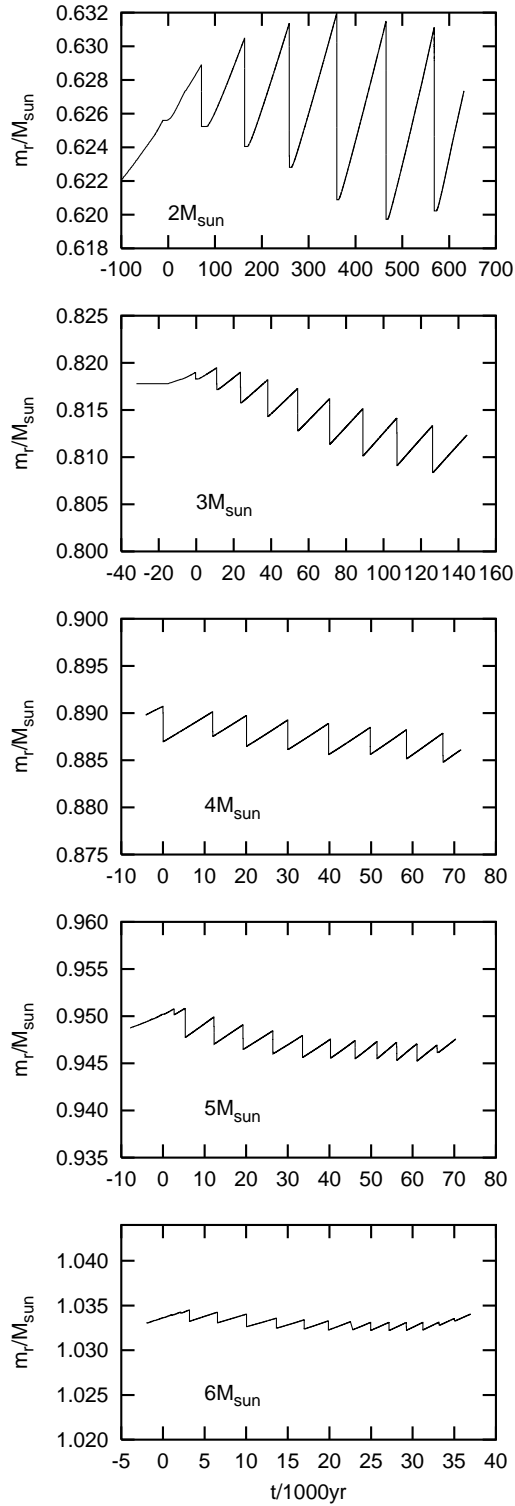


Fig. 3.— Core mass evolution. All panels show the same mass range of  $\Delta m_r = 0.025 M_{\odot}$ .

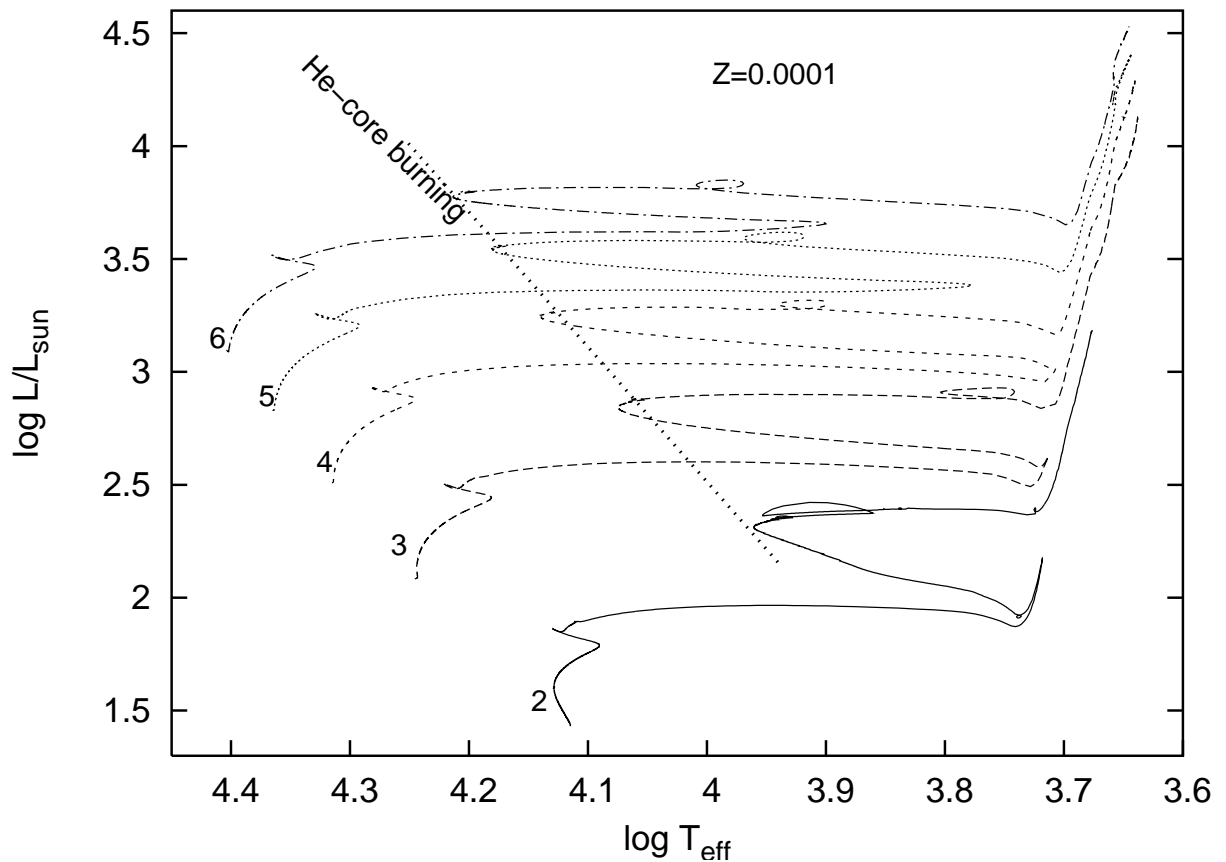


Fig. 4.— HRD for the pre-AGB evolution. The numeric labels indicate the initial stellar mass of the tracks. Note that higher-mass cases do not possess a RGB evolution phase.

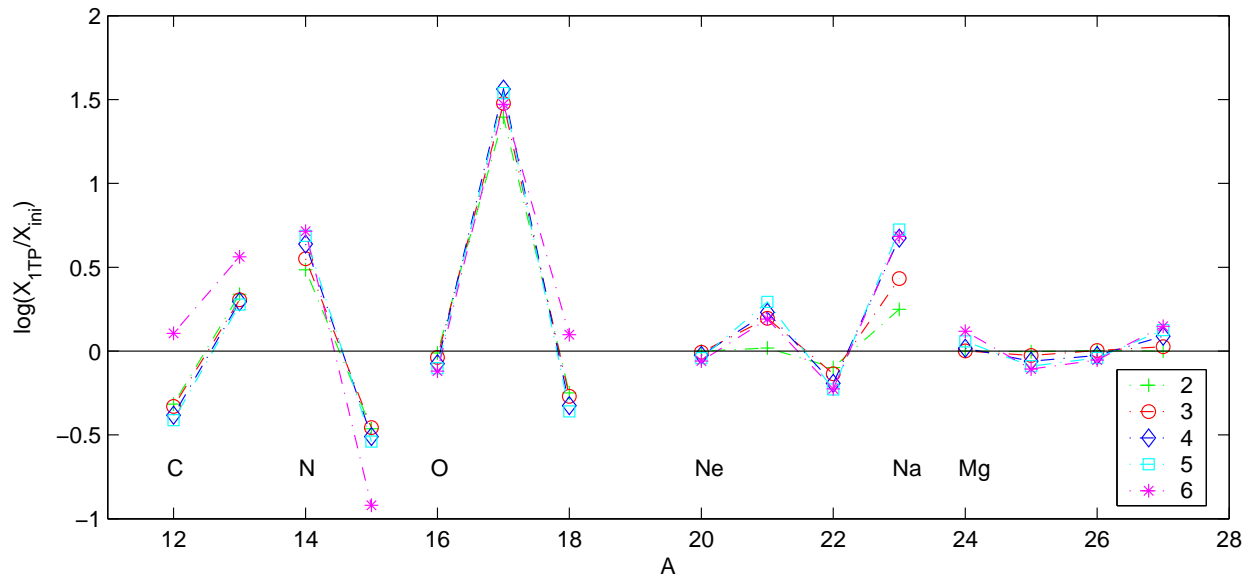


Fig. 5.— Overabundances in the envelope just before the first TP, caused by the second dredge-up, and in the  $2 M_{\odot}$  case through the first DUP.  $X_{\text{ini}}$  is the solar-scaled initial abundance. Lines connect isotopic abundances for the respective stellar mass of the elements C, N and O, and for the Ne-Na and Mg-Al groups. EDITOR: THIS FIGURE DOUBLE COLUMN PLEASE

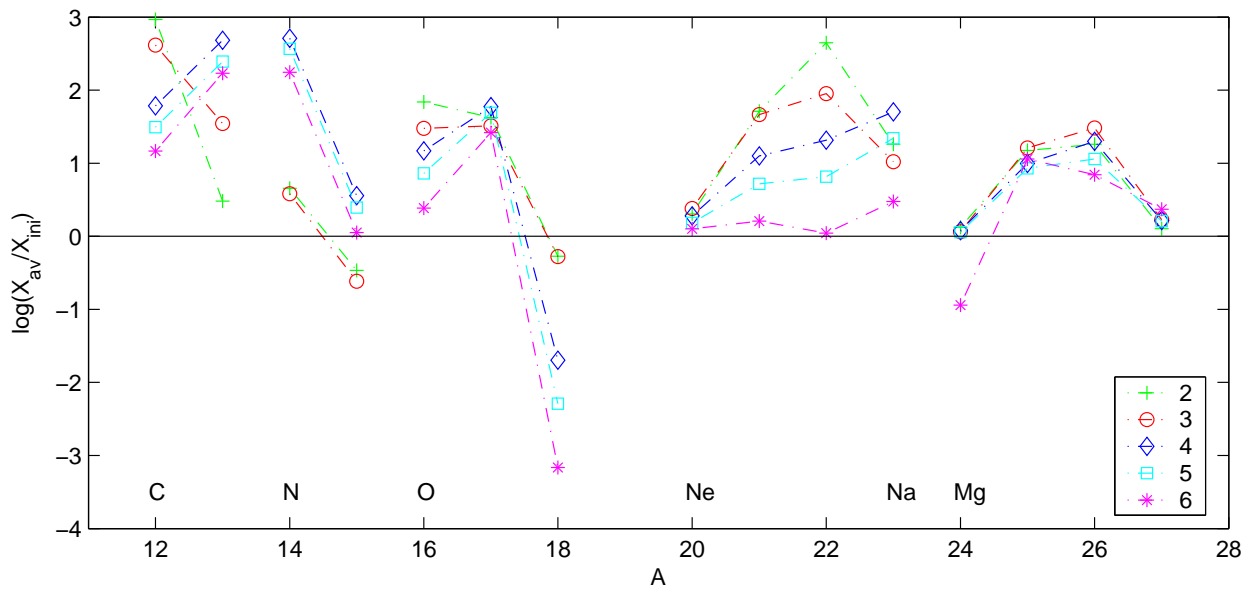


Fig. 6.— Overabundances of CNO and Ne-Al isotopes in material returned to ISM.  $X_{\text{ini}}$  is solar-scaled and thus for each species  $\log(X_{\text{av}}(I)/X_{\text{ini}}) = [\text{I}/\text{Fe}]$ , where the square brackets have their usual meaning of the logarithmic abundance ratio relativ to the solar ratio. Lines connect isotopic abundances for the respective stellar mass of the elements C, N and O, and for the Ne-Na and Mg-Al groups. EDITOR: THIS FIGURE DOUBLE COLUMN PLEASE

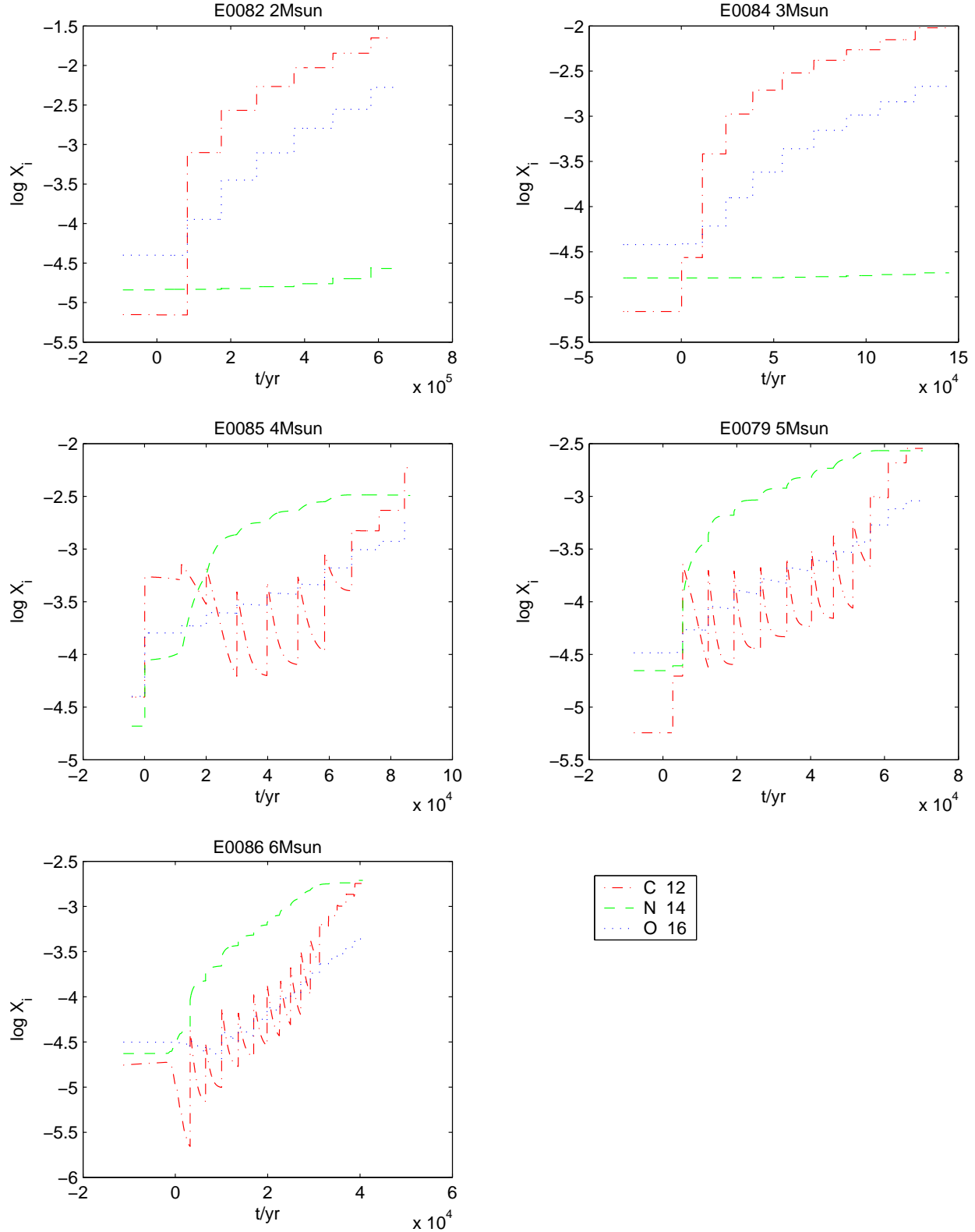


Fig. 7.— Abundance evolution of the most abundant CNO isotopes for all sequences during the TP-AGB.

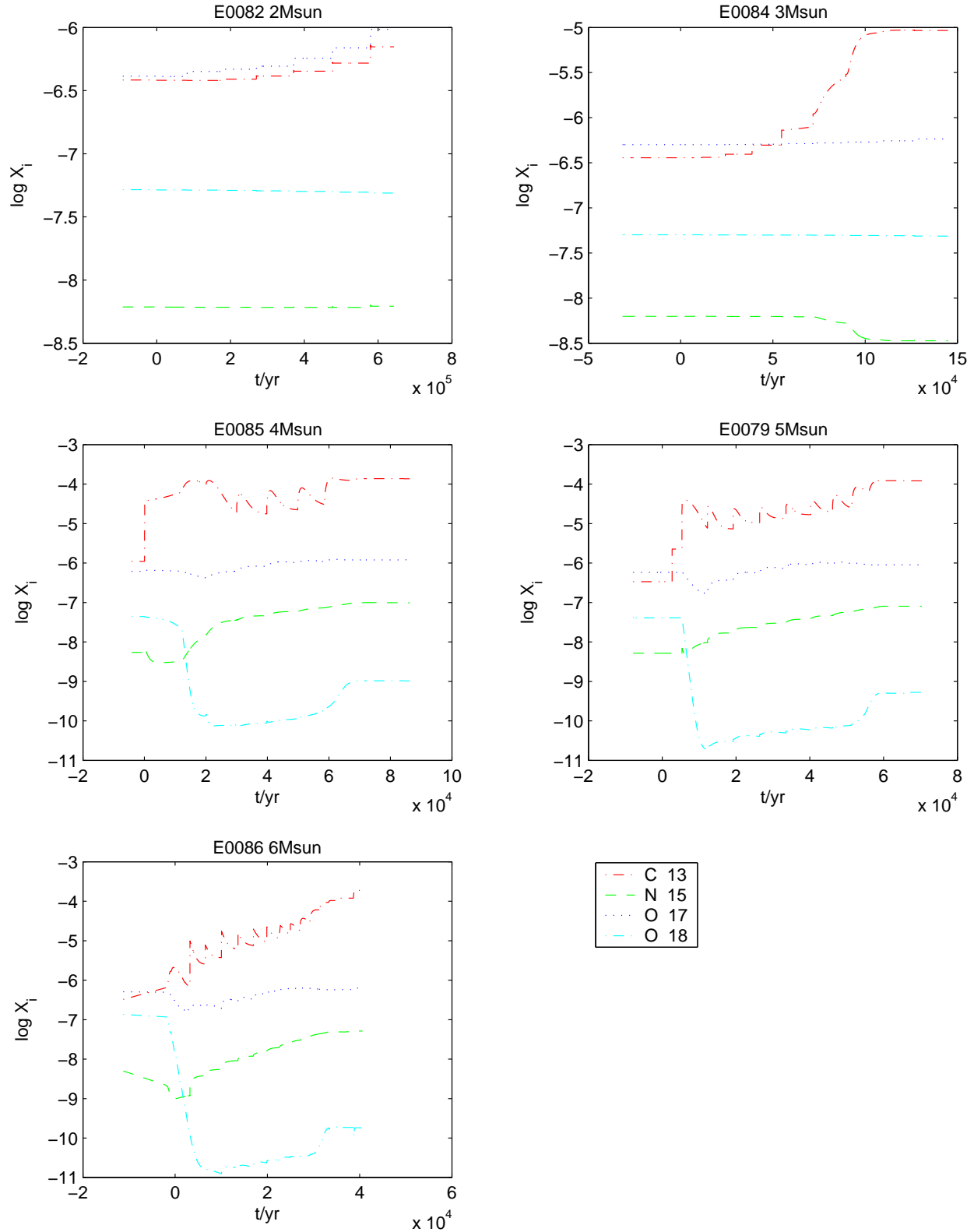


Fig. 8.— Abundance evolution of the less abundant CNO isotopes.

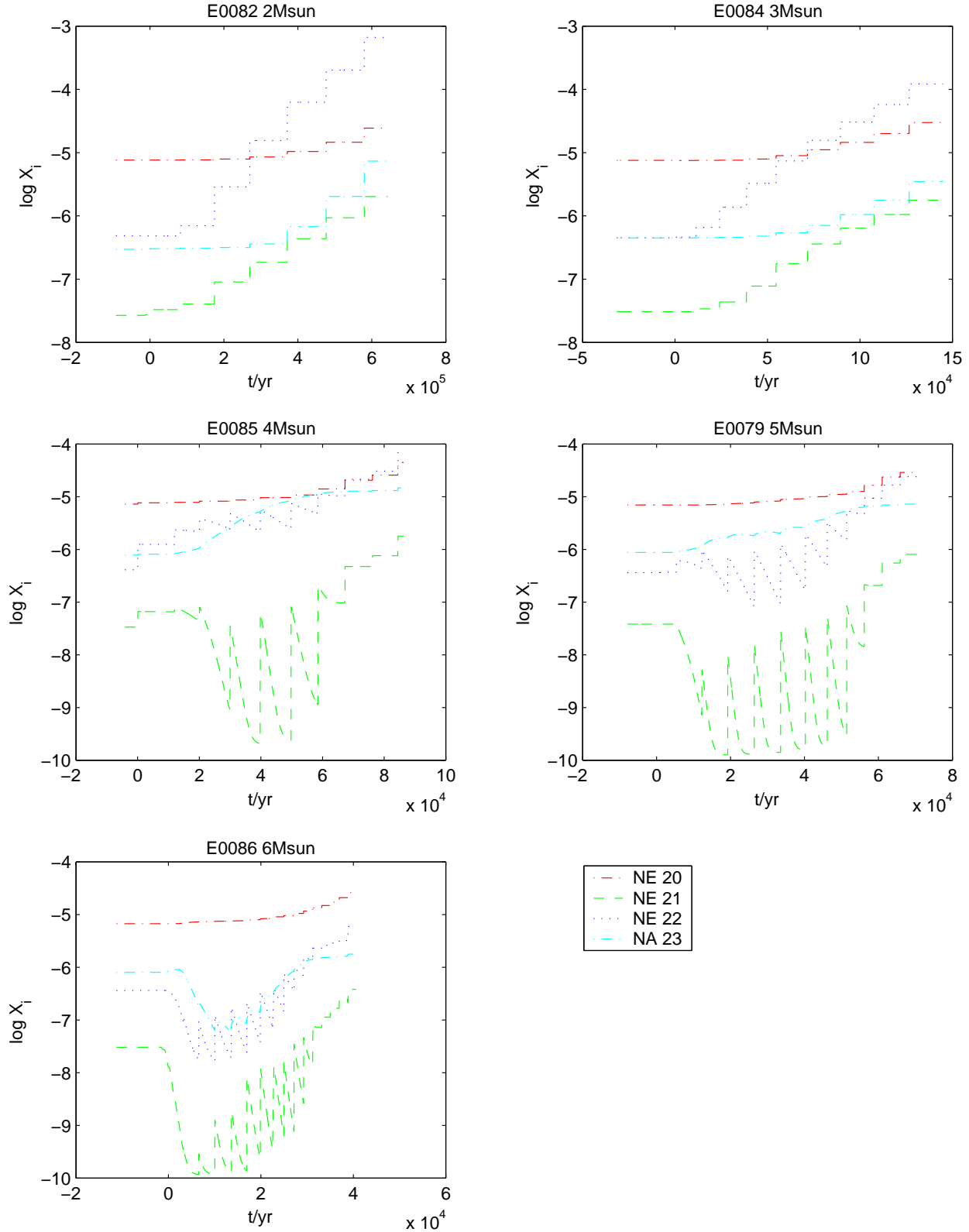


Fig. 9.— Abundance evolution of the stable Ne and Na isotopes for all sequences during the TP-AGB evolution.

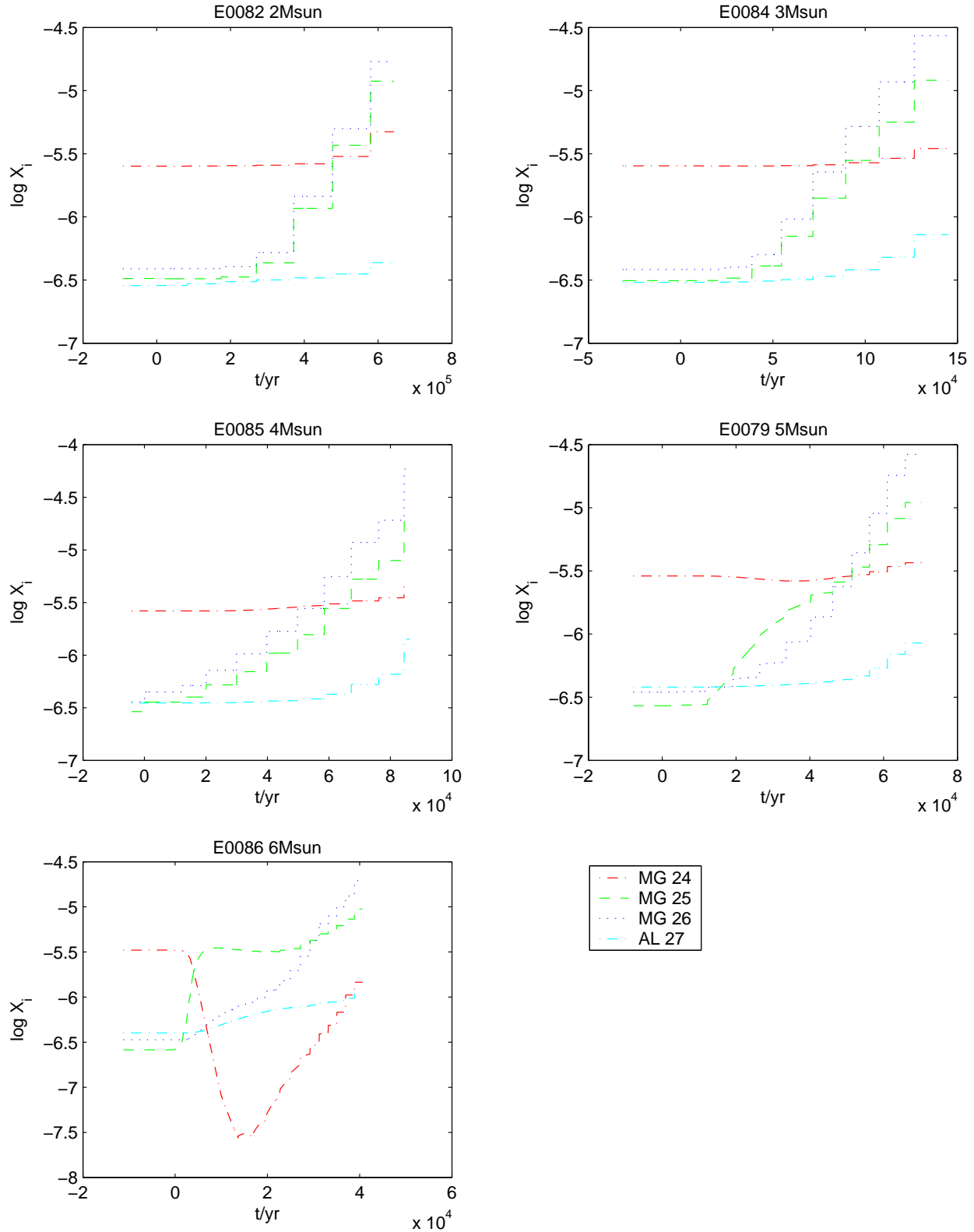


Fig. 10.— Abundance evolution of the stable Mg and Al isotopes for all sequences during the TP-AGB evolution.

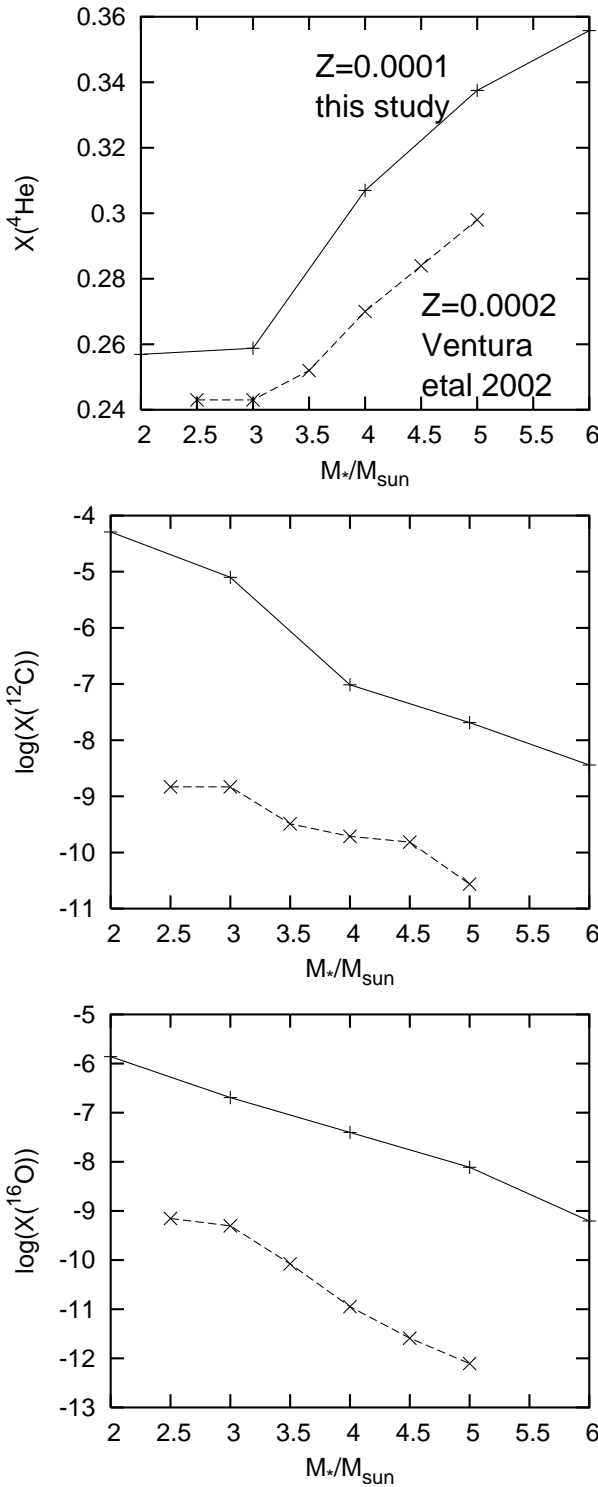


Fig. 11.— Average mass fractions in ejected material according to this study compared to (Ventura et al. 2002). Apart from a small difference in metallicity the main difference is in dredge-up efficiency as a result of mixing assumptions (see text for details).